

**Male pheromones modulate synaptic transmission at the *C. elegans*
neuromuscular junction in a sexually dimorphic manner**

Kang-Ying Qian^{1,4,5}, Wan-Xin Zeng^{1,4,5}, Yue Hao^{1,4,5}, Xian-Ting Zeng¹, Haowen Liu⁸, Lei Li⁸,
Lili Chen⁹, Fu-min Tian¹, Cindy Chang^{6,7}, Qi Hall^{6,7}, Chun-Xue Song^{2,3}, Shangbang Gao⁹,
Zhi-Tao Hu⁸, Joshua M Kaplan^{6,7}, Qian Li^{2,3,*} and Xia-Jing Tong^{1,10,*}

¹School of Life Science and Technology, ShanghaiTech University, Shanghai 201210, China.

²Center for Brain Science, Shanghai Children's Medical Center, Shanghai Jiao Tong
University School of Medicine, Shanghai 200127, China.

³Department of Anatomy and Physiology, Shanghai Jiao Tong University School of Medicine,
Shanghai 200025, China.

⁴Institute of Neuroscience, Shanghai Institutes for Biological Sciences, Chinese Academy of
Sciences, Shanghai 200031, China.

⁵University of Chinese Academy of Sciences, Beijing 100190, China.

⁶Department of Molecular Biology, Massachusetts General Hospital, Boston, MA 02114,
USA.

⁷Department of Neurobiology, Harvard Medical School, Boston, MA 02115, USA

⁸Queensland Brain Institute, Clem Jones Centre for Ageing Dementia Research (CJCADR),
The University of Queensland, Brisbane, QLD 4072, Australia

⁹College of Life Science and Technology, Huazhong University of Science and Technology,
Wuhan, 430074, China.

¹⁰Lead Contact

*Correspondence: liqian@shsmu.edu.cn (Q.L.), tongxj@shanghaitech.edu.cn (X-J.T.)

SUMMARY

The development of functional synapses in the nervous system is important for animal physiology and behaviors, and its disturbance has been linked with many neurodevelopmental disorders. The synaptic transmission efficacy can be modulated by the environment to accommodate external changes, which is crucial for animal reproduction and survival. However, the underlying plasticity of synaptic transmission remains poorly understood. Here we show that in *C. elegans*, the male environment increases the hermaphrodite cholinergic transmission at the neuromuscular junction (NMJ), which alters hermaphrodites' locomotion velocity and mating efficiency. We identify that the male-specific pheromones mediate this synaptic transmission modulation effect in a developmental stage-dependent manner. Dissection of the sensory circuits reveals that the AWB chemosensory neurons sense those male pheromones and further transduce the information to NMJ using cGMP signaling. Exposure of hermaphrodites to the male pheromones specifically increases the accumulation of presynaptic CaV2 calcium channels and clustering of postsynaptic acetylcholine receptors at cholinergic synapses of NMJ, which potentiates cholinergic synaptic transmission. Thus, our study demonstrates a circuit mechanism for synaptic modulation and behavioral flexibility by sexual dimorphic pheromones.

Keywords: synaptic transmission, neuromuscular junction (NMJ), acetylcholine receptor, CaV2 calcium channel, pheromone, chemosensory neuron, sexual dimorphism

INTRODUCTION

Faithful synaptic transmission is essential for animal physiology and behaviors. The disturbance of synaptic transmission has been linked with several neurodevelopmental disorders, including autism spectrum disorders (ASD). In the past decades, researchers have identified numerous genes encoding synaptic proteins that are linked with neurodevelopmental disorders, and their mutations cause the dysregulated synaptic transmission in human diseases (Doan et al., 2016; Doan et al., 2019; Geisheker et al., 2017; Iossifov et al., 2012; Lee et al., 2019; Morrow et al., 2008; Neale et al., 2012; Yuen et al., 2017), including *SHANK3*, *NRXN*, and *NLGN* for autism (Chen et al., 2020; Lee et al., 2015; Levinson and El-Husseini, 2005; Orefice et al., 2019; Sudhof, 2008), *MECP2* for Rett's syndrome (Chao et al., 2007; Orefice et al., 2019), *FMR1* for Fragile X syndrome (Olmos-Serrano et al., 2010), and *UBE3* for Angelman syndrome (Judson et al., 2016; Wallace et al., 2012).

The process of synaptogenesis occurs in the early postnatal developmental period, and can be modulated by the environment. The effects of synaptic modulation could persist until adulthood and cause a lifelong impact. Various environmental contexts can modulate synaptic transmission and behaviors through experience-dependent plasticity, which provides a critical and conserved mechanism to generate animal behavior diversity and adaption. Among the environmental contexts, social interaction, such as the density of the conspecifics sharing the same habitat, represents one of the most important environmental conditions that modulate animal physiology and behaviors to meet the ever-changing environment and internal needs (Chen and Hong, 2018). For example, social isolation of rats during the critical period of adolescence enhances long-term potentiation of NMDA receptor-mediated glutamatergic transmission in the ventral tegmental area (Whitaker et al., 2013). Besides that, maternal separation has been found to have a profound lifelong influence on animal models at a mature stage of life. It causes habenula hyperexcitability, AMPA receptors delivery, and synaptic plasticity defects in the developing barrel cortex (Miyazaki et

al., 2012; Tchenio et al., 2017). However, the underlying mechanism on how social interaction modulates synaptic transmission remains elusive.

There are many ways in which social interaction can influence neural development. Pheromone effects between conspecifics are strong drivers that modulate behaviors and alter physiology, allowing appropriate responses to particular social environments (Liberles, 2014). These effects are often sexually dimorphic. Mouse pups elicit parental care behaviors in virgin females, for instance, but promote infanticidal behaviors in virgin males through pheromonal compounds (submandibular gland protein C and hemoglobins) and physical traits (Isogai et al., 2018). In *C. elegans*, a family of glycolipids called ascarosides function as the pheromones to mediate social interactions. Males and hermaphrodites secrete several ascarosides in different amounts that elicit sexual dimorphic responses (Butcher et al., 2007; Edison, 2009; Greene et al., 2016; Srinivasan et al., 2008; Srinivasan et al., 2012). For example, the male-enriched ascr#10 induces attraction behavior in hermaphrodites, but causes aversion behavior in males (Izrayelit et al., 2012). However, it remains unclear whether and how specific pheromone-mediated effects are involved in neurodevelopmental processes, including synaptogenesis and synaptic transmission.

Here, we show that the male environment increases the cholinergic synaptic transmission at the neuromuscular junction (NMJ) in *C. elegans* hermaphrodites, decreasing hermaphrodite's locomotion activity and promotes mating efficiency. The male-specific pheromones (ascarosides) mediate these effects in a sexually dimorphic manner. Such ascaroside-mediated modulation of the cholinergic synaptic transmission is developmental stage-dependent. We further used various neuron-type-specific ablation experiments to confirm that these male-specific pheromone signals are received and processed by the AWB chemosensory neuron pair in hermaphrodites. Upon reception, AWB neurons transduce the information to the NMJ using cGMP signaling. Furthermore, we used multiple reporter fusion constructs to show that the male-specific pheromones cause increased calcium channel accumulation and acetylcholine receptor (AChR) clustering at cholinergic synapses. Collectively, our work elucidates how individuals sense and adapt to the social environment,

providing insights into how pheromones regulate the development and function of the nervous system.

RESULTS

The male environment modulates synaptic transmission at the hermaphrodite NMJ

C. elegans has two sexes: XX hermaphrodites and XO males. The somatically female hermaphrodites can produce hermaphrodite progeny by self-fertilization (although rare males are generated through spontaneous X chromosome loss), whereas in the presence of males, they are also able to mate with males to give rise to equal ratios of hermaphrodites and males (Figure 1A). Hermaphrodites generated by self-fertilization or by crossing share the same genetic background but develop in distinct environments (*i.e.*, in the presence or absence of males). Therefore, it provides an excellent system to study how social interaction modulates the establishment and maintenance of synaptic transmission during development. We selected the *C. elegans* NMJ as a model to examine the male environment's effects on synaptic transmission. The *C. elegans* NMJ includes body-wall muscles that receive synaptic inputs from both excitatory cholinergic and inhibitory GABAergic motor neurons (Richmond and Jorgensen, 1999). The coordination of excitatory and inhibitory innervations guarantees *C. elegans* sinusoidal movement. In the presence of acetylcholinesterase inhibitors such as aldicarb, the breakdown of acetylcholine is prevented, and acetylcholine accumulates over time at synapses. As a result, worms become paralyzed due to hyper-excitation (Mahoney et al., 2006). The timing of the paralysis is influenced by the inhibitory innervations from GABAergic neurons that counteract acetylcholine's excitatory effect and delay paralysis. The percentage of paralyzed worms over time can be used as a measurement of excitatory versus inhibitory synaptic transmission ratio (E/I ratio) at the NMJ. As a result, the alteration of sensitivity to aldicarb reflects the changes in NMJ synaptic transmission (Vashlishan et al., 2008).

To determine whether the NMJ synaptic transmission differs between hermaphrodites generated through self-fertilization versus crossing, we applied aldicarb to

young adult hermaphrodites and examined the percentage of paralyzed animals. We found that around 39.8% of hermaphrodites from self-fertilization were paralyzed after 70 minutes' exposure to aldicarb. In contrast, almost all of the hermaphrodites from crossing were paralyzed (Figure 1B), indicating that hermaphrodites obtained by crossing are more sensitive to aldicarb. Thus, the NMJ E/I ratio is increased in crossed hermaphrodites than those obtained by self-fertilization.

There are three possible explanations for the observed differences in NMJ synaptic transmission in crossed hermaphrodites: first, it could be a parental inheritance effect, such as RNA transgenerational transmission (Alcazar et al., 2008; Rechavi et al., 2011); second, it could be caused by direct contact with males (Shi and Murphy, 2014); third, male metabolites secreted into the environment could modulate hermaphrodite development. To rule out the potential effects of parental inheritance and male contact, we directly exposed hermaphrodites from self-fertilization to medium conditioned by either the male or the hermaphrodite environment since egg stage. The conditioned medium was prepared by collecting cultures of *him-5* mutants containing around 40% males (male-conditioned medium) or wild type hermaphrodites alone (hermaphrodite-conditioned medium). Both conditioned media contain metabolites secreted by 30,000 young adult worms during three-hour cultivation (Figure 1C). After growing hermaphrodites in the conditioned medium, we found that the hermaphrodites cultured in the male-conditioned medium became paralyzed earlier than those in the hermaphrodite-conditioned medium (80.31% vs. 61.11% paralyzed after 70 minutes' exposure to aldicarb) (Figure 1D). This result suggests that the effect of the male environment on hermaphrodite NMJ is mediated by male-secreted metabolites. In the following experiments, we directly used the male-conditioned medium and hermaphrodite-conditioned medium unless otherwise specified.

We then analyzed muscle excitability as another independent measure of synaptic transmission changes at the NMJ. Previous work has shown that the body-wall muscle at the *C. elegans* NMJ receives both excitatory and inhibitory inputs from cholinergic and GABAergic neurons, respectively (Richmond and Jorgensen, 1999). When the excitatory

and inhibitory synaptic transmission ratio increases at the NMJ, the excitability of muscle cells should increase. To verify the increased excitability of the body-wall muscle, we expressed the genetically encoded calcium indicator GCaMP3 in muscle cells (under the *myo-3* promoter) and the channelrhodopsin variant Chrimson in VB and DB motor neurons (under the *acr-5* promoter) (Figure 1E) (Tian et al., 2009). Fluorescence changes reflect calcium influx and excitability in the GCaMP3-expressing cells. We found that the baseline GCaMP3 fluorescence is higher in hermaphrodites grown in the male-conditioned medium compared with those grown in the hermaphrodite-conditioned medium, suggesting relatively higher resting muscle excitability (Figure 1-figure supplement 1). Moreover, we excited the VB and DB cholinergic motor neurons via optogenetic activation of Chrimson with red light (wavelength at 640 nm) (Klapoetke et al., 2014), and observed significantly increased GCaMP3 fluorescence intensity potentiation (assessed as $\Delta F/F$) in hermaphrodites grown in the male-conditioned medium (Figure 1F-G). These results indicate that the male excretome environment causes increased excitatory and inhibitory synaptic transmission ratio and muscle excitability at the NMJ of hermaphrodites.

The acetylcholine transmission rate at the NMJ is potentiated by the male excretome environment

The increased E/I ratio could be caused by either increased cholinergic transmission or decreased GABAergic transmission. To distinguish between these two possibilities, we analyzed spontaneous miniature excitatory postsynaptic currents (mEPSCs) and miniature inhibitory postsynaptic currents (mIPSCs) at the NMJ. We found that the mEPSC frequency was significantly increased in hermaphrodites from male-conditioned medium compared to those from hermaphrodite-conditioned medium (Figure 1H-I), but the mEPSC amplitude was not changed (Figure 1H, 1J). When we examined inhibitory postsynaptic currents, we detected no significant differences in mIPSC frequency and amplitude between hermaphrodites from male- or hermaphrodite-conditioned medium (Figure 1K-M). The

electrophysiology data suggest that potentiation of acetylcholine transmission rate mainly contributes to the observed increase in the E/I ratio at the NMJ of hermaphrodites in the male excretome environment.

The male excretome environment increases the hermaphrodite NMJ synaptic transmission during the juvenile stage

To delineate if there are any critical developmental windows for the observed synaptic transmission modulation by the male environment, we transferred hermaphrodites to male-conditioned medium at a series of different developmental stages (egg, L1 [24 hours after egg], L2-L3 [36 hours after egg], and mid-L4 [48 hours after egg]). We then measured synaptic transmission in young adults with the aldicarb assay (Figure 2A). The hermaphrodites transferred to the male-conditioned medium at the egg, L1, and L2-L3 stage presented significantly increased sensitivity to aldicarb when they grow into young adult (Figure 2B and Figure 2-figure supplement 1A-C, 92.5% vs. 55.1% at 70 minutes for egg stage, 46.9% vs. 24.9% for the L1 stage, and 71.3% vs. 14.0% for L2-L3 stage). In contrast, we observed no differences in sensitivity to aldicarb between hermaphrodites transferred to male-conditioned medium at the mid-L4 stage and those from hermaphrodite-conditioned medium (Figure 2B and Figure 2-figure supplement 1D, 15.9% vs. 14.0% at 70 minutes). Those data suggest that exposure to the male excretome environment in L3-L4 stage is critical for modulation of the NMJ synaptic transmission in hermaphrodites.

To study whether the sustained male environment is required to maintain the cholinergic synaptic transmission potentiation at NMJ, we removed hermaphrodites from male-conditioned medium out of the male environment at L4 (48 hours after egg) and young adult (60 hours after egg). 24 and 12 hours later, we performed the aldicarb assay (Figure 2A, 2C, and Figure 2-figure supplement 1E). We found that hermaphrodites leaving the male excretome environment at the young adult stage still showed an increased sensitivity to aldicarb compared with those in the hermaphrodite-conditioned medium (66.3% vs. 42.0% at 70 minutes). The effect was comparable to that in hermaphrodites sustained in the male

environment (78.0% vs. 42.0%) (Figure 2C), suggesting that the maintenance of the elevated cholinergic synaptic transmission rate at the hermaphrodites NMJ does not require a sustained male excretome environment in adults. In contrast, we observed that the hermaphrodite leaving the male-conditioned medium at the mid-L4 stage presented similar aldicarb sensitivity to those from the hermaphrodite-conditioned medium (37.7% vs. 42.0% at 70 min) (Figure 2C and Figure 2-figure supplement 1E). Taken together, these data support the notion that the male environment exposure at a critical period (the L3-L4 stage) is required for the modulation of hermaphrodites NMJ cholinergic synaptic transmission.

The aforementioned experiments were carried out using the Bristol N2 strain. To determine whether the male excretome environment's effect is conserved in other *C. elegans* strains, we studied several natural variations, including the Australian strain AB3, the Hawaiian strain CB4856, and the Madison strain TR389. We observed that the male-conditioned medium accelerated animal paralysis in the CB4856 (Figure 2D, 59.7% vs. 20.7% after 60 minutes of aldicarb) and the AB3 strains (Figure 2E, 52.8% vs. 28.6% after 80 minutes of aldicarb), but not in the TR389 strain (Figure 2F, 68.46% vs. 60.99% after 130 minutes of aldicarb). Thus, although the effect of the male environment does exist in other natural *C. elegans* strains, exceptions do exist, as in the TR389 strain.

Two possibilities could account for this lack of a modulator effect: TR389 males may not be able to secrete the modulator ascarosides; alternatively, TR389 hermaphrodites cannot sense and respond to the modulator ascarosides. To distinguish between these two possibilities, we grew Bristol N2 hermaphrodites in the TR389 male-conditioned medium and compared their synaptic transmission by aldicarb sensitivity with those maintained in N2 and TR389 hermaphrodite-conditioned medium. The three groups presented similar sensitivity to aldicarb (Figure 2G). In contrast, TR389 hermaphrodites grown in the N2 male-conditioned medium showed significantly increased sensitivity to aldicarb compared to those in the N2 hermaphrodite-conditioned medium (Figure 2-figure supplement 2). Thus, TR389 males appear unable to secrete the modulator ascarosides.

The male excretome environment alters hermaphrodite locomotion and promotes mating efficiency

As mentioned above, the coordination of excitatory and inhibitory innervations at NMJ guarantees *C. elegans* sinusoidal movement. To study whether the altered cholinergic synaptic transmission impacts body-bend amplitude and coordination of animal movement, we compared the locomotion of hermaphrodites from male- or hermaphrodite-conditioned medium. We observed that males had higher body curvature and locomotor velocity than hermaphrodites (Figure 2-figure supplement 3A-B), consistent with previous studies (Mowrey et al., 2014). We did not observe body-bend curvature differences in hermaphrodites from male- and hermaphrodite-conditioned medium (Figure 2-figure supplement 3C-D). However, the locomotor velocities of hermaphrodites from male-conditioned medium are significantly lower than those from hermaphrodite-conditioned medium (Figure 2H). In contrast, the TR389 male-conditioned medium did not show similar effects (Figure 2H). This supports the notion that the altered NMJ synaptic transmission by the male excretome affects hermaphrodite locomotion. It's possible that the disturbance of excitatory and inhibitory synaptic transmission balance at NMJ compromise locomotion activity.

Communications between conspecifics modulate behaviors and alter physiology to allow appropriate responses to particular social environments. To study the physiological significance of male excretome modulation, we tested its effect on hermaphrodite's egg-laying behaviors and mating abilities. We calculated the brood size of hermaphrodites from hermaphrodite- and male-conditioned medium, and observed no significant differences between the two groups (Figure 2-figure supplement 4). Then we measured the mating efficiency with males in hermaphrodites from male- and hermaphrodite-conditioned medium. Two young adult stage hermaphrodites from male- or hermaphrodite-conditioned medium were cultured with two young-adult males for 24 hours. Successful mating was scored when more than 3 male progenies were generated in the mating plate. The results showed that hermaphrodites from TR389 male-conditioned medium had higher mating efficiency

compared to those from hermaphrodite-conditioned medium (Figure 2I), which is consistent with previous research that the male environment reduces hermaphrodite exploration and increases mating behaviors (Aprison and Ruvinsky, 2019a, b). Interestingly, we found that N2 male-conditioned medium showed a significant further increase of hermaphrodite mating efficiency than the TR389 male-conditioned medium (Figure 2I). We speculate that the N2 males secrete additional metabolites to modulate locomotion and mating efficiency in hermaphrodites.

Male-specific ascarosides mediate the modulatory effect of the male excretome environment on the hermaphrodite NMJ synaptic transmission

To identify the additional metabolites secreted by the N2 males, we focused on searching the male pheromones. In *C. elegans*, ascarosides are known to function as pheromones to mediate social interactions and modulate development (Butcher et al., 2007; Butcher et al., 2009; Ludewig et al., 2019; Ludewig and Schroeder, 2013; Srinivasan et al., 2008; Wu et al., 2019). We hypothesized that the observed effects of the male environment on hermaphrodite cholinergic synaptic transmission at the NMJ may be mediated by male-specific ascarosides. Ascarosides are derivatives of 3,6-dideoxysugar ascarylose, and their biosynthesis requires several dehydrogenases, including DAF-22, which β -oxidizes and shortens long-chain fatty acids to generate bioactive medium- and short-chain ascarosides (Figure 3A) (Butcher et al., 2009; von Reuss et al., 2012; Zhou et al., 2018). Therefore, most of the active short- and medium-chain ascarosides are absent from the metabolomes of *daf-22* mutants (Butcher et al., 2009; von Reuss et al., 2012; Zhou et al., 2018).

To test if the effect of the male environment on hermaphrodite NMJ synaptic transmission is mediated by ascarosides, we grew hermaphrodites in *daf-22* conditioned medium and compared their aldicarb sensitivity to hermaphrodites grown in the wild type conditioned medium. We found that the hermaphrodites grown in the *daf-22* male-conditioned medium exhibited similar aldicarb sensitivity with those grown in *daf-22*

hermaphrodite-conditioned medium (Figure 3B, 43.7% vs. 43.7% at 70 minutes). The inability of the *daf-22* male environment to modulate hermaphrodite NMJ synaptic transmission suggests that male-specific ascarosides do contribute to the observed modulatory effects on synaptic transmission.

The pheromone effects are often sexually dimorphic. To study whether the male-specific ascarosides also modulate male NMJ synaptic transmission, we compared the aldicarb sensitivity of males grown in the hermaphrodite- and male-conditioned media. We did not observe aldicarb sensitivity differences in males from hermaphrodite- and male-conditioned medium (Figure 3-figure supplement 1A). Since males can secrete those modulatory pheromones themselves, we took advantage of *daf-22* mutant males that have the defects in pheromone production. We also found that *daf-22* males from the male-conditioned medium did not show any significant differences in aldicarb sensitivity compared to those from the hermaphrodite-conditioned medium (Figure 3C). In contrast, the *daf-22* hermaphrodites showed higher aldicarb sensitivity from the male-conditioned medium compared to those from the hermaphrodite-conditioned medium (Figure 3-figure supplement 1B), suggesting *daf-22* mutation did not alter the modulatory effect of male-conditioned medium on hermaphrodites. These results indicate that male-specific ascarosides cannot modulate synaptic transmission in males, suggesting a sexually dimorphic effect of those male-specific ascarosides.

The *C. elegans* ascarosides comprise a complex mixture of ascaroside derivatives that vary according to their side-chains; there are saturated, α,β -unsaturated (e.g., α,β double bond), and β -hydroxylated (e.g., β -hydroxylated side chain) derivatives. Hermaphrodites and males are known to accumulate distinct types and quantities of these various ascarosides (Butcher et al., 2009; von Reuss et al., 2012). To identify the “modulator ascarosides” that function in the observed modulation of the hermaphrodite NMJ synaptic transmission, we first analyzed the TR389 strain, which recalls appearing unable to secrete the modulator ascarosides.

To further determine the identity of the modulator ascarosides, we used Ultra Performance Liquid Chromatography-Mass Spectrometry (UPLC-MS) analyses to compare the excretomes among N2 hermaphrodite cultures (containing N2 hermaphrodites only), N2 male cultures, *daf-22* male cultures, and TR389 male cultures (all of the male cultures contains around 35% males) (Figure 3D). We collected and analyzed culture media samples with UPLC-MS and found that ascr#10 was enriched in both the N2 male and TR389 male cultures relative to the N2 hermaphrodite cultures (Figure 3-figure supplement 2A), consistent with previous reports (Izrayelit et al., 2012). We also observed that the *daf-22* male cultures lacked most of the short- and medium-chain ascarosides, and accumulated the long-chain ascarosides (Figure 3-figure supplement 2B), confirming the role of DAF-22 in dehydrogenating and shortening ascaroside side chains.

Next, reasoning that the modulator ascarosides should be enriched in N2 male-conditioned culture, we compared the UPLC-MS profiles of N2 male cultures with the N2 hermaphrodites and the TR389 male cultures. The medium-chain β -hydroxylated ascarosides were substantially increased in the N2 male cultures compared to the N2 hermaphrodite cultures and TR389 male cultures. Specifically, the significantly enriched β -hydroxylated ascarosides in N2 males included C13, C14, and C15 ascarosides (Figure 3E). Notably, we detected no significant changes between the N2 and TR389 male cultures for saturated ascarosides (Figure 3-figure supplement 2C). These results implicate that the medium-chain β -hydroxylated ascarosides may act as the male modulator ascarosides.

Pursuing this with a genetic approach, we acquired a mutant of the known ascaroside synthesis enzyme DHS-28; previous analysis of the *dhs-28* mutant hermaphrodite metabolome has shown that these animals accumulate β -hydroxylated medium-chain ascarosides (Butcher et al., 2009; von Reuss et al., 2012). We conducted aldicarb assays to compare the E/I ratios of *dhs-28* cultures with those of N2 hermaphrodites grown in the hermaphrodite-conditioned medium. As expected, *dhs-28* mutant hermaphrodites were more sensitive to aldicarb compared with N2 hermaphrodites (Figure

3F). We also tested hermaphrodites of other known ascaroside synthesis mutants, including *maoc-1* and *acox-1.1*—which are known to accumulate saturated and α,β -unsaturated side-chain ascarosides—but found that *maoc-1* mutants present slightly increase of aldicarb sensitivity than the wild type, and *acox-1.1* mutants were indifferent from the wild type for their sensitivity to aldicarb (Figure 3F). Furthermore, we examined the male ascaroside effects on *dhs-28* mutants, which could accumulate β -hydroxylated medium-chain ascarosides themselves. The result showed that *dhs-28* hermaphrodites cannot be modulated by male ascarosides by presenting comparable aldicarb sensitivity when in hermaphrodite- and male-conditioned medium (Figure 3G). These experiments with ascaroside biosynthesis mutants establish that environmental enrichment of β -hydroxylated medium-chain ascarosides increases the hermaphrodite NMJ E/I ratio, thereby supporting that these specific ascarosides may function as NMJ cholinergic synaptic transmission modulators.

AWB sensory neurons are involved in sensing the modulator ascarosides and transmit signals to the NMJ through cGMP signaling

Pheromone signals in the environment are detected and integrated by chemosensory neural circuits (Ludewig and Schroeder, 2013; Srinivasan et al., 2008). In *C. elegans*, there are 11 pairs of chemosensory neurons that can respond to pheromone signals (ASE, AWC, AWA, AWB, ASH, ASI, ADF, ASG, ASJ, ASK, and ADL). To identify the specific chemosensory neurons sensing the modulator ascarosides, we used a miniSOG (mini Singlet Oxygen Generator)-induced genetic ablation strategy. miniSOG is an engineered fluorescent protein that can generate singlet oxygen upon blue light illumination. Targeting miniSOG to mitochondria can lead to singlet oxygen accumulation in mitochondria, which induces rapid and efficient cell death (Qi et al., 2012). To examine the genetic ablation efficiency, we co-expressed mCherry and miniSOG in the chemosensory neurons under the control of the *flp-21* promoter and quantified the miniSOG ablation efficiency based on the

percentage of live neurons labeled by mCherry before and after induction of cell death. To optimize the ablation protocol, we tested continuous blue light stimulation at a power of 57 mW/cm² over different periods (Figure 4-figure supplement 1A). We found that 15 minutes' stimulation resulted in complete loss of mCherry signals in around 47.8% of neurons and a dramatic reduction of mCherry signals in 26.1% of neurons, whereas stimulation for 30 minutes or 50 minutes led to complete loss of mCherry signals in almost 80% of neurons and faint residual expression of mCherry signals in 20% of neurons (Figure 4-figure supplement 1B-C). Considering both the ablation efficiency and the stimulation time, we chose 30 minutes of continuous blue light stimulation for our standard ablation procedure.

We screened all the 11 pairs of chemosensory neurons based on miniSOG-induced genetic ablation of hermaphrodites at the late L1 stage (Figure 4A). We grew hermaphrodites in male-conditioned or hermaphrodite-conditioned medium following ablation of each specific chemosensory neuron type, and measured their sensitivity to aldicarb. Ablation of the AWB (*str-1* promoter driving miniSOG) neuron pair in hermaphrodites blocked the increased sensitivity to aldicarb following exposure to the male-conditioned medium (Figure 4B-C, 45.6% vs. 43.4% at 80 minutes). In contrast, the increased aldicarb sensitivity in the male-conditioned medium remained when any other chemosensory neurons were ablated (Figure 4A and Figure 4-figure supplement 2A-G). To further confirm the requirement of AWB in sensing the modulator ascarosides, we compared the locomotion of AWB-ablated hermaphrodites from male- and hermaphrodite-conditioned medium. Our data showed that ablation of AWB neurons decreased the locomotion velocity in hermaphrodites from the hermaphrodite-conditioned medium. In addition, ablation of AWB neurons blocked the decreased velocity by the modulator ascarosides (Figure 4D). These results support that AWB neurons in hermaphrodites are necessary for the effects of male-specific modulator ascarosides on NMJ synaptic transmission.

We also tested whether activation of AWB neurons is sufficient to modulate NMJ synaptic transmission. We specifically expressed the channelrhodopsin variant CHIEF in AWB neurons, and administered blue light illumination in the presence of all-trans retinal

(ATR) to activate AWB neurons throughout the L4 stage. We observed decreased aldicarb sensitivity in animals fed with ATR (ATR+ light- vs. ATR- light-). Nevertheless, hermaphrodites with activated AWB neurons during the L4 stage showed higher sensitivity to aldicarb than controls without blue light activation (ATR+ light+ vs. ATR+ light-) (Figure 4E). This effect is absent in the groups lacking ATR (ATR- light+ vs. ATR- light-) (Figure 4E). In contrast, activation of ASJ/ASI neurons or other amphid wing neurons like AWA and AWC cannot increase aldicarb sensitivity, and the hermaphrodites with AWA neurons activation even present slightly decreased aldicarb sensitivity (Figure 4-figure supplement 3). These findings confirm that activation of the AWB chemosensory neuron pair in hermaphrodites is sufficient to modulate the NMJ synaptic transmission.

In order to test whether AWB neurons directly sense those modulator ascarosides, we monitored intracellular Ca^{2+} dynamics upon male excretomes stimulation by expressing the calcium indicator GCaMP6f in AWB neurons. We found that the AWB neurons elicited a rapid and robust calcium transient responding to the male excretomes. However, no responses were detected by stimulation with the hermaphrodite excretomes (Figure 4F-H). Collectively, the data support that AWB neurons directly respond to the male-specific modulator ascarosides.

We next explored which signaling molecules in AWB neurons mediate their responsivity to the modulator ascarosides. In *C. elegans*, most chemical odors are perceived upon their binding to specific G-protein coupled receptors (GPCRs) located in chemosensory neurons; these receptors subsequently activate downstream signaling cascades (Bargmann, 2006; Li and Liberles, 2015; Liberles, 2014). The G protein ODR-3 and the cGMP-gated channels TAX-2 have been implicated in chemosensory signal transduction in AWB neurons. We first examined the NMJ E/I ratio in *tax-2* and *odr-3* mutant hermaphrodites. We observed no differences in sensitivity to aldicarb for *tax-2* mutant hermaphrodites upon exposure to the male-conditioned or hermaphrodite-conditioned media (Figure 4I). In the *odr-3* mutants, we even observed a decreased aldicarb sensitivity in hermaphrodites from male-conditioned medium (Figure 4J), suggesting that the ability to

mediate the downstream signaling effects of modulator ascarosides and increase NMJ E/I ratio is disrupted in these mutants (Figure 4I, 4J). Further supporting this, complementing TAX-2 expression in AWB neurons rescued the increased aldicarb sensitivity phenotype of hermaphrodites grown in the male-conditioned medium (Figure 4I). Expression of TAX-2 in ASI and ASJ neurons had no such rescue effect (Figure 4I). The increased sensitivity to aldicarb was also rescued by ODR-3 complementation in AWB neurons (Figure 4J). Together, these results establish that the cGMP signaling pathway in AWB chemosensory neurons transmits male-specific modulator ascaroside signals to the NMJ.

Excitatory postsynaptic receptor clustering is increased in hermaphrodites exposed to the male environment

The steps of the synaptic transmission process include presynaptic vesicle fusion, neurotransmission, and neurotransmitter binding to postsynaptic receptors. The increased cholinergic synaptic transmission rate at the hermaphrodite NMJ induced by the modulator ascarosides could reflect changes in any of these steps. We first examined whether any NMJ synaptic structures were altered, specifically by labeling cholinergic synapses via expression of a RAB-3-GFP fusion protein in DA and DB cholinergic motor neurons (using the *unc-129* promoter) (Colavita et al., 1998). DA and DB neurons are known to receive synaptic inputs in the ventral nerve cord and to form NMJs with the body-wall muscle in the dorsal nerve cord, and this results in the formation of puncta comprising presynaptic RAB-3 proteins that can be observed at DA/DB axon terminals in the dorsal cord (Colavita et al., 1998). We observed that puncta fluorescence intensities and densities were comparable in hermaphrodites grown in either hermaphrodite- or male-conditioned medium (Figure 5A), which suggested that the excitatory synapse structures were unaltered by the presence of modulator ascarosides. We next labeled the GABAergic motor neuron terminals by expressing RAB-3 fused with RFP under the *unc-25* promoter (Jin et al., 1999). Similar to the excitatory cholinergic synapses, the puncta fluorescence intensities and densities in the inhibitory GABAergic synapses did not differ between hermaphrodites from male-conditioned

or hermaphrodite-conditioned medium (Figure 5B), which collectively suggest that neither excitatory nor inhibitory synapse structures are affected by the modulator ascarosides.

We then examined the extent of excitatory and inhibitory postsynaptic receptor localization in hermaphrodites by analyzing the subcellular distributions of nicotinic acetylcholine receptors (nAChRs; excitatory) and GABA_A receptors (inhibitory). A single-copy transgenic insertion technique was applied to express fluorescence reporter fusion variants of two known nAChR subunit proteins (UNC-29-RFP and ACR-16-RFP) or a GABA_A receptor subunit (UNC-49-mCherry) under the control of a muscle-specific promoter. At cholinergic synapses, the hermaphrodites from the male-conditioned medium had a slight but significant increase in puncta signal intensities for the nAChRs compared to those from the hermaphrodite-conditioned medium (Figure 5C-D). However, the GABA_AR intensities were not changed (Figure 5E). Both the nAChRs and GABA_AR densities were unaltered (Figure 5C-E). Thus, the male-specific modulator ascarosides are involved in increased postsynaptic receptor abundance at excitatory synapses in hermaphrodites.

Presynaptic CaV2 calcium channel localization at NMJ cholinergic synapses is increased in hermaphrodites exposed to the male environment

Next, we examined if the process of presynaptic neurotransmission is regulated based on the fact that the mEPSC frequency was increased in hermaphrodites by the male-specific pheromones (Figure 1H-J). N-type voltage-gated calcium channels (CaV2) are required for the presynaptic calcium influx process that underlies both excitatory and inhibitory neurotransmission (Liu et al., 2018; Tong et al., 2017). Therefore, we inspected CaV2 calcium channel localization and abundance at presynaptic elements in hermaphrodites grown in either hermaphrodite- or male-conditioned medium. To visualize endogenous CaV2 at excitatory or inhibitory synapses separately, we utilized the split GFP complementary system (Cabantous et al., 2005; Kamiyama et al., 2016). In *C. elegans*, UNC-2 encodes the CaV2 calcium channel α subunit, and we used CRISPR/Cas9 system to

insert a sequence coding for seven GFP11 fragments at the C-terminus of UNC-2/CaV2. In parallel, the GFP 1-10 fragment was constitutively expressed in DA and DB cholinergic motor neurons under the control of the *unc-129* promoter or in the GABAergic motor neurons under the control of the *unc-47* promoter (Figure 6A). In this way, we were able to monitor the endogenous localization of CaV2 channels at excitatory and inhibitory synapses. To validate the correct subcellular localization, we coexpressed the presynaptic marker UNC-57/Endophilin fused with mCherry. The CaV2-GFP fusion protein formed fluorescent puncta largely co-localized with UNC-57/Endophilin in dorsal cord axons (Figure 6B-C, Pearson correlation coefficient 0.7808 ± 0.022 for DA/DB cholinergic motor terminals, and 0.7880 ± 0.0175 for GABAergic motor neuron terminals), confirming that CaV2-splitGFP is localized correctly at presynaptic elements. We further found that UNC-57/Endophilin fluorescence intensities and densities were indistinguishable in hermaphrodites from the hermaphrodite- and male-conditioned medium (Figure 6-figure supplement 1). This result is consistent with RAB-3-GFP imaging results, and support that the presynaptic structure is not altered by male pheromone (Figure 5A-B).

Comparison of the CaV2 puncta fluorescence intensities revealed a significant increase at cholinergic synapses of hermaphrodites from male-conditioned medium compared to those from the hermaphrodite-conditioned medium (Figure 6D). A slight but notable increase in densities was also observed (Figure 6D). In contrast, we detected no significant differences in CaV2 puncta fluorescence intensities and densities at GABAergic synapses (Figure 6E).

To further confirm that CaV2 is the synaptic target of modulator ascarosides, we compared the cholinergic synaptic transmission and locomotion velocity in *unc-2* hermaphrodites from male- and hermaphrodite-conditioned medium. The mEPSC rate and locomotion velocity in the *unc-2* mutant were decreased compared to those in the wild type (Figure 7A-B), which is correlated with the requirement of CaV2 in mediating presynaptic transmission. Furthermore, we found that the male-specific ascarosides no longer increase

mEPSC rates in the *unc-2* hermaphrodites (Figure 7A-C). Similarly, the locomotion velocity was not changed in *unc-2* hermaphrodites from male-condition medium compared to those from hermaphrodite-condition medium (Figure 7D), which suggests that *unc-2* mutation blocks the effects of the male-specific modulator ascarosides on NMJ synaptic transmission. These findings collectively indicate that the male-specific modulator ascarosides may promote the accumulation of CaV2 calcium channels at excitatory cholinergic synapses, accounting for the potentiated cholinergic synaptic transmission at NMJ.

DISCUSSION

In this study, we have revealed a novel mechanism through which the male environment modulates the NMJ synaptic transmission, locomotion behavior, and mating efficiency in hermaphrodites. We show that the male environment effects are mediated based on exposure to male-specific pheromones at a specific developmental stage in hermaphrodites (the entire L3-L4 stage). We further demonstrate that hermaphrodite sense and process these male-specific pheromones by AWB chemosensory neurons using the cGMP signaling. At the hermaphrodite NMJ, presynaptic calcium channel localization and postsynaptic acetylcholine receptor clustering are elevated by exposure to male-specific pheromones, resulting in an increased cholinergic synaptic transmission. Our results provide mechanistic details of how environmental factors alter neuronal development and physiology, presenting insights to better understand the associations between dysregulated neurodevelopment and various psychiatric diseases.

***C. elegans* NMJ as a model to study synaptogenesis**

Here, we used the *C. elegans* NMJ as a model to study synaptic transmission, and our work underscore *C. elegans* as a useful model to study synaptic transmission *in vivo*. The motor circuit of *C. elegans* relies on a precise balance between cholinergic excitation and GABAergic inhibition of body-wall muscles to generates precise locomotion activities (Richmond and Jorgensen, 1999). Both our and others' studies have identified mechanisms

of synaptogenesis and synaptic transmission that are shared by the *C. elegans* NMJ and the mammalian central nervous system (Dolphin and Lee, 2020; Hata et al., 1993; Ogawa et al., 1998; Pevsner et al., 1994; Richmond et al., 1999; Rizo and Sudhof, 2012). In the worm motor circuit and the mammalian brain, acetylcholine is an excitatory neurotransmitter while GABA is an inhibitory neurotransmitter. Moreover, the clustering of acetylcholine receptors and GABA receptors at synapses is observed in *C. elegans* and vertebrates (Maro et al., 2015; Pouloupoulos et al., 2009; Tong et al., 2015; Tu et al., 2015).

It is also highly notable that many autism-linked synaptic proteins, including Neuroligins and Neurexins, have been shown to function with conserved roles in NMJ synaptogenesis and synaptic transmission (Hart and Hobert, 2018; Hu et al., 2012; Kurshan et al., 2018; Philbrook et al., 2018; Tong et al., 2017): Neuroligins and Neurexins form trans-synaptic complex and regulate synaptic transmission in both mammalian central nervous system and *C. elegans* NMJ (Hu et al., 2012; Kurshan et al., 2018; Tong et al., 2017). Neuroligins are required for postsynaptic GABA_A-receptor clustering and inhibitory synaptic transmission (Maro et al., 2015; Pouloupoulos et al., 2009; Tong et al., 2015; Tu et al., 2015). While Neurexins undergo ectodomain shedding by ADAM10 protease (Borcel et al., 2016; Tong et al., 2015), bind to presynaptic CaV2 calcium channel $\alpha 2\delta$ subunits, and regulate calcium channel activity (Luo et al., 2020; Tong et al., 2017). Thus, the mechanisms we identified here in the *C. elegans* NMJ may provide new insights into how synaptic transmission is maintained in the mammalian brain.

Sexual dimorphic modulation on NMJ synaptic transmission

We show that a previously unknown circuit comprised of AWB chemosensory neurons regulates NMJ synaptic transmission in *C. elegans*. Interestingly, the male-enriched pheromones increase the acetylcholine transmission specifically in hermaphrodites but not in males, suggesting sexual dimorphism in the regulation of NMJ synaptic transmission. This could be mediated by sex-specific neuronal circuits that are composed of either sex-specific

or sex-shared neurons to process and transmit male pheromone signals to NMJ. A *C. elegans* male has 385 neurons, whereas a hermaphrodite has 302 neurons. The majority of male-specific neurons are localized in the male tail and are involved in the complex mating behaviors. There are several hermaphrodite-specific neurons in the nervous system, including VC and HSN motor neurons, which are mainly required for reproductive functions (Banerjee and Hallem, 2018; Emmons, 2018; Garcia and Portman, 2016). On the other hand, several sex-shared neurons, including motor neurons, AWA, AWC, and ASK chemosensory neurons, DVA mechanosensory neurons, as well as AVA interneurons, could contribute to sex-specific neural circuits by mediating attraction and aversion behaviors (Banerjee and Hallem, 2018; Bayer and Hobert, 2018; Cook et al., 2019; Fagan et al., 2018; Mowrey et al., 2014; Narayan et al., 2016; Wan et al., 2019). Our results identified that AWB chemosensory neurons mediate a sexually dimorphic modulation of NMJ synaptic transmission. Further studies will be required to unravel the downstream neural circuits, including interneurons and premotor neurons, that function to process the modulator ascaroside signals to modulate NMJ synaptic transmission. Another possibility for this sexual dimorphic modulation is from sexually dimorphic hormone signaling pathways, such as vasopressin/oxytocin and their receptors (Garrison, 2012).

Our data show that pheromones modulating hermaphrodite NMJ synaptic transmission are enriched in N2 males. Previous studies have reported various male-specific ascarosides, including ascr#10 and indole containing ascarosides (IC-ascarosides, especially icas#3 and icas#9). However, our data indicate that ascr#10 and indole IC-ascarosides are unlikely the modulator ascarosides. First, ascr#10 levels are comparable in N2 and TR389 males. Second, previous work has established that ASI and ASK sensory neurons are required for hermaphrodites to sense ascr#10 and IC-ascarosides (Aprison and Ruvinsky, 2017; Dong et al., 2016), whereas we find that ASI and ASK neurons are dispensable for hermaphrodites to sense the modulator ascarosides. In contrast, our UPLC-MS data strongly suggest that the medium-chain β -hydroxylated ascarosides (C13, C14, and

C15) may mediate this effect. Although we provided extensive genetic evidence, we have not experimentally confirmed that these specific ascarosides are sufficient to modulate hermaphrodite NMJ synaptic transmission.

Previous studies by Brunet and Murphy labs have shown that male pheromone exposure affects animal health and shortens hermaphrodite life span (Maures et al., 2014; Shi and Murphy, 2014; Shi et al., 2017). Here our data suggest that it might be different mechanisms to modulate longevity and NMJ synaptic transmission. In previous research, they found that exposure of hermaphrodite to male pheromones at the beginning of their life (day 1) or sexual maturity (day 4) had a similar effect on hermaphrodites' life span. However, we showed that L3-L4 is a critical developmental stage for modulation of hermaphrodite NMJ synaptic transmission by male pheromones (Figure 2A-C). Distinct male-specific pheromones may mediate the effects on longevity and NMJ. Further studies should be carried out to identify the specific ascaroside pheromones in males.

Our work demonstrates that early pheromone environment exposure has a long-term effect on synaptic transmission. We suspect that the observed effects may be mediated through endocrine signaling pathways, such as DAF-7/TGF- β and DAF-2/insulin, which are known to drive both epigenomic and transcriptional changes. In this light, recent studies have shown how pheromone exposure can inhibit learning behavior by disrupting the balance between two insulin-like peptides, ins-16 and ins-4 (Wu et al., 2019). Further studies are required to characterize whether endocrine system components like insulin signaling molecules are involved in regulating synaptic transmission in response to male-specific ascarosides.

Presynaptic calcium channels as neuromodulation targets

Our results show that modulator pheromones regulate hermaphrodite NMJ cholinergic transmission by altering the presynaptic localization of calcium channel CaV2 at cholinergic synapses. These results support that CaV2 calcium channels can be viewed as

potential targets for environmental modulation of the synaptic transmission. At synapses, CaV2 channels are known to form large signaling complexes in the presynaptic nerve terminal that are responsible for calcium influx and neurotransmitter release (Dolphin and Lee, 2020). Numerous studies have verified causal relationships for calcium channel mutations and polymorphisms in neuropsychiatric diseases, including ASD (Nanou and Catterall, 2018; Zamponi, 2016). Our previous studies identified a synaptic retrograde signal mediated by autism-linked proteins that regulate CaV2 presynaptic localization to alter excitatory synaptic transmission (Tong et al., 2017). Here, we present the important evidence that the presynaptic calcium channel CaV2 could also be a target of social interaction modulation to shift the synaptic excitation and inhibition balance. These results support the idea that changes in presynaptic calcium channel localization could be impactful in some forms of ASD.

How might changes in chemosensory neuron activity contribute to presynaptic calcium channel localization? Our results suggest that it is not a general change of CaV2 expression levels, because we observed increased presynaptic localization at cholinergic synapses but not at GABAergic synapses. We suspect that the specific synaptic recruitment of CaV2 is somehow potentiated by the modulator ascarosides. Previous studies have suggested that protein interactions are required for cell-surface localization of calcium channels as well as their docking at the active zone. It is therefore possible that pre-synapse specific proteins that are only present at cholinergic synapses may act downstream of the chemosensory circuits to regulate the surface localization of CaV2 channels.

Collectively, our findings reveal a novel mechanism through which pheromones in the environment modulate synaptogenesis and synaptic transmission in the nervous system. Beyond suggesting that calcium channels may be a shared target for both genetic and environmental modulation during development, our study lays a foundation for studies into the signaling and cell-specific functions underlying neurodevelopmental dysfunction.

ACKNOWLEDGEMENTS

We thank the *C. elegans* Genetics Stock Center, National BioResource Project (NBRP), Jean-Louis Bessereau, Yingchuan Billy Qi, and Quan Wen for sharing strains and reagents. We also thank the Molecular Imaging Core Facility (MICF), Biological Mass Spectrometry Core Facility (BMSCF) at School of Life Science and Technology, ShanghaiTech University for help in calcium imaging and mass spectrometric analysis. This work was supported by the Basic Research Project from the Science and Technology Commission of Shanghai Municipality (19JC1414100 to X-J.T.), National Natural Science Foundation of China (31741054 to X-J.T.), Shanghai Pujiang Program (18PJ1407600 to X-J.T. and 17PJ1405400 to Q.L.), Shanghai Brain-Intelligence Project from the Science and Technology Commission of Shanghai Municipality (18JC1420302), Program for Special Appointment at Shanghai Institutions of Higher Learning (QD2018017 to Q.L.), Innovative research team of high-level local universities in Shanghai, National Institute of Neurological Disorder and Stroke (NS32196 to J.M.K.), National Institutes of Health research grant (NEI 1R21EY029450-01 to J.L. and Z.H.), and National Health and Medical Research Council (APP1122351 to Z.H.).

MATERIALS AND METHODS

Key Resources Table				
Reagent type (species) or resource	Designation	Source or reference	Identifiers	Additional information
strain, strain background (<i>C.elegans</i>)	<i>C. elegans</i> strains used in this study are listed in Supplementary File 1			
Strain (Escherichia coli)	OP50	CGC	RRID: WB-STRAIN:OP50	

sequence-based reagent	Sequence information is listed in Supplementary File 2			
recombinant DNA reagent	pPD49.26	Addgene (Andrew Fire)	https://www.addgene.org/1686/	
recombinant DNA reagent	pPD95.75	Addgene (Andrew Fire)	https://www.addgene.org/1494/	
recombinant DNA reagent	pCFJ910	Addgene (Erik Jorgensen)	https://www.addgene.org/44481/	
recombinant DNA reagent	CZ14527	Yingchuan B. Qi	Qi, Y. B et al., 2012	Plasmid: Punc-17β::tomm-20N::miniSO G
recombinant DNA reagent	quan0071	Quan Wen	Xu, T et al., 2018	Plasmid: Pacr-5::chromson
recombinant DNA reagent	pSG368	Shangbang Gao	Gao, S et al., 2018	Plasmid: GCaMP6f
commercial assay or kit	PureLink® HiPure Plasmid Miniprep Kit	Invitrogen	Cat#: K210002	

commercial assay or kit	QIAprep Spin Miniprep Kit	Qiagen	Cat#: 27106	
commercial assay or kit	PrimeSTAR Max DNA Polymerase	Takara	Cat#: R045A	
commercial assay or kit	hyPerFusion™ high-fidelity DNA polymerase	ApexBio	Cat#: K1032	
commercial assay or kit	Hieff CLONE™ Plus One Step Cloning Kit	Yeasten	Cat#: 10911ES62	
chemical compound, drug	Aldicarb	ApexBio	Cat#: B4778	
chemical compound, drug	All-trans- Retinal	Sigma	Cat#: R2500	
chemical compound, drug	Geneticin, G418 Sulfate	GOLDBIO	Cat#: G-418-1	
chemical compound, drug	2,3- Butanedione monoxime	Sigma	Cat#: B0753	

chemical compound, drug	Polybead® Microspheres 0.10 µm	Polysciences	Cat#: 00876-15	
chemical compound, drug	Fluospheres carboxylat	Life Science	Cat#: F8813	
software, algorithm	ImageJ	NIH	https://imagej.nih.gov/ij/download.html	
software, algorithm	Igor pro 6.3	WaveMetrics	https://www.wavemetrics.com/products/igorpro/igorpro.htm	
software, algorithm	GraphPad Prism 8	GraphPad	https://www.graphpad.com/scientific-software/prism/	
software, algorithm	MATLAB	MathWorks	https://www.mathworks.com/products/matlab.html?s_tid=hp_products_matlab	
software, algorithm	MetaMorph	Molecular Devices	https://www.moleculardevices.com/systems/metamorph-research-imaging/metamorph-microscopy-automation-and-image-analysis-software	
software, algorithm	WormLab	MBF Bioscience	https://www.mbfbioscience.com/wormlab	

CONTACT FOR REAGENT AND RESOURCE SHARING

Further information and requests for resources and reagents should be directed to and will be fulfilled by the Lead Contact Xia-Jing Tong (tongxj@shanghaitech.edu.cn).

EXPERIMENTAL MODEL AND SUBJECT DETAILS

Animals

C. elegans were maintained under standard conditions at 20 °C on plates made from nematode growth medium (NGM). *E. coli* OP50 was used as a food source for all experiments except where HB101 *E. coli* was utilized for electrophysiology study. A description of all alleles can be found at <http://www.wormbase.org/#012-34-5>. Animals were obtained from Bristol variety N2 strain unless specially indicated. Transgenic animals were prepared by microinjection, and integrated transgenes were isolated following UV irradiation or by miniMos insertion.

Plasmids

All worm expression vectors were modified versions of pPD49.26 (A. Fire) or miniMos vector pCFJ910. Standard methods and procedures were utilized for all of the plasmids. A 3.1 kb *ceh-36* promoter was used for expression in ASE and AWC chemosensory neurons. A 3 kb *odr-10* promoter was used for expression in AWA chemosensory neurons. A 3 kb *str-2* promoter was used for expression in AWC chemosensory neurons. A 3 kb *str-1* promoter was used for expression in AWB chemosensory neurons. A 3 kb *srb-6* promoter was used for expression in ADF, ADL, and ASH chemosensory neurons. A 3 kb *gpa-4* promoter was used for expression in ASI chemosensory neurons. A 3 kb *gcy-15* promoter was used for expression in ASG chemosensory neurons. A 3.9 kb *sra-7* promoter was used for expression in ASK chemosensory neurons. A 4.1 kb *flp-21* promoter was used for expression in the majority of the chemosensory neurons. A 4.3 kb *acr-5* promoter was used for expression in DB and VB motor neurons. A 2.4 kb *myo-3* myosin promoter was used for expression in body muscles. For rescue experiments, *TAX-2* (F36F2.5.1), *ODR-3*

(C34D1.3.1), and *ACR-16* (F25G6.3) were amplified from the N2 cDNA library using gene-specific primers.

Generation of single-copy insertion allele by homologous recombination

The xjSI0002 allele encoding RFP-tagged *ACR-16* minigene under the muscle-specific *myo-3* promoter was generated by miniMOS (Frokjaer-Jensen et al., 2014). The RFP sequence was inserted between the third and the fourth transmembrane segment of *ACR-16*.

Aldicarb assay

The aldicarb assay was performed as previously described (Vashlishan et al., 2008). Aldicarb (ApexBio) was dissolved in ethyl alcohol and added to NGM at a final concentration of 1.4mM (Testing hermaphrodites) or 0.5 mM (Testing males). These plates (35mm) were seeded with 75 ul OP50 and allowed to dry overnight before use. More than 20 animals at the young adult stage (otherwise indicated) were picked on an aldicarb plate for aldicarb assay. Animals were scored as paralyzed when they did not respond to the platinum wire prodding. The paralyzed animals were counted every 10 or 15 minutes. At least three double-blind replicates for each group were tested.

Preparation of conditioned media

Hermaphrodite and male-secreted metabolites were collected according to a previous publication (Srinivasan et al., 2008). Synchronized *C. elegans* (WT [N2], *him-5* [N2], WT [TR389], *him-5* [TR389], *daf-22* [N2], and *daf-22; him-5* [N2]) with a density of 10,000 worms/plates (90 mm, three plates) were grown on the nematode growth media (NGM) agarose (seeded with *E. coli* strain OP50) at 20 °C. There were $43.07 \pm 0.77\%$, $39.26 \pm 1.55\%$, and $37.29 \pm 1.28\%$ males in *him-5* (N2), *daf-22; him-5* (N2), and *him-5* (TR389) strains respectively. After worms reached the young adult stages, they were collected and washed three times with M9 buffer to remove bacteria. To further remove the bacteria in the gut, the worms were then placed in M9 buffer in a shaker (150 rpm) at 20 °C for 30 minutes,

and rinsed three times with ddH₂O. Subsequently, worm-secreted metabolites were collected by incubating the worms in ddH₂O in a shaker (150 rpm) for 3 hours with a density of 30,000 worms/ml. Afterward, the worms were removed by settling on ice for 5 minutes. The metabolites were filtered through 0.22 µm filters, aliquoted and stored at -80 °C. For conditioned medium preparation, 10 µl metabolites mixed with 90 µl OP50 *E. coli* were spread on a 35 mm NGM plate. Plates were allowed to dry overnight before use.

Calcium imaging

Muscle calcium responses were measured by detecting fluorescence intensity changes of GCaMP3. *C. elegans* expressing GCaMP3 in the body-wall muscle (*Pmyo-3::GCaMP3*) and Chrimson in the DB and VB neurons (*Pacr-5::Chrimson*) were used for calcium imaging experiments. Young adult animals fed with 1.6 mM ATR (in 100 µl *E. coli* OP 50) were immobilized on 10% agarose pads by polystyrene microbeads. Fluorescence images were captured using a Nikon 60x 1.4 NA objective on a Nikon spinning-disk confocal system (Yokogawa CSU-W1) at 10 ms per frame. We used wide-field illumination with a nominal wavelength at 640 nm for Chrimson activation. The GCaMP signals were captured using 488 nm laser excitation and were analyzed by ImageJ software.

Calcium responses in the soma of AWB sensory neurons were measured by detecting fluorescence intensity changes of GCaMP6f. A home-made microfluidic device was used for calcium imaging as previously described (Liu et al., 2019; Zou et al., 2018). Briefly, a young adult animal was rinsed by M9 buffer and loaded into a home-made microfluidic device with its nose exposed to buffer under laminar flow. Diluted metabolites of N2 hermaphrodite and *him-5* mutants was delivered using a programmable automatic drug feeding equipment (MPS-2, InBio Life Science Instrument Co. Ltd, Wuhan, China). For Ca²⁺ fluorescence imaging in AWB, the neurons were exposed under fluorescent excitation light for 30 seconds before recording, to eliminate the light-evoked calcium transients. During the recording process, for the first 5 seconds, we gave the M9 solution then switched hermaphrodite excretome or male excretome for 30 seconds, removing extract liquid from

35 second and washing for 25 seconds. The AWB neurons were imaged with a 60X objective (Olympus) and EMCCD camera (Andor iXonEM) at 100 ms/frame. The imaging sequences were subsequently analyzed using Image-Pro Plus6 (Media Cybernetics, Inc., Rockville, MD, USA).

Adult locomotion analysis

To analyze adult locomotor behavior, young adult worms were washed with M9 buffer before transferred to the unseeded NGM plate, and allowed to recover for 5 minutes. Animal locomotion was recorded at a rate of 10 frames per second (fps) for 1 minute. The mean body-bend amplitude and crawling locomotion velocity were analyzed by WormLab. All the assays were done at 25 °C.

Mating behaviors

Mating efficiency was assessed as previously described (Yin et al., 2017). Briefly, two young adult stage hermaphrodites from male- or hermaphrodite-conditioned medium were cultured with two young-adult males for 24 hours. Successful mating was scored when more than 3 male progenies were generated in the mating plate. Mating efficiency was obtained by calculating the percentage of successful mating in more than 15 plates.

Liquid culture and mass spectrometric analysis

The crude pheromone extracts were prepared according to a previously published protocol (Zhang et al., 2013). N2 wild type, *him-5* mutant, *daf-22*; *him-5* mutant or TR389 *him-5* mutant worms were grown for two generations on 60 mm NGM plate seeded with *E.coli* OP50 bacteria. Worms from four plates were washed by M9 buffer and cultured in 50 ml S complete medium (100 mM NaCl, 50 mM KPO₄, 3 mM CaCl₂, 3 mM MgSO₄, 5 µg/mL Cholesterol, 10 mM Potassium citrate, 50 µM disodium EDTA, 25 µM FeSO₄, 10 µM MnCl₂, 10 µM ZnSO₄, 1 µM CuSO₄) at 20 °C and 200 rpm. The animals were cultured with shaking

at 200 rpm for 7 days (around 30,000 worms/ 50 ml). 25X Concentrated *E.coli* OP50 bacteria were supplemented every day (0.3 ml for day 1, 1 ml for day 2-5, and 2 ml for day 6-7). After 7 days, the supernatant medium containing metabolites was collected by centrifugation (3,000 g, 10 minutes). Then the supernatant media were frozen at -80 °C, lyophilized, and extracted with methanol for UPLC-MS (Ultra Performance Liquid Chromatography) analysis. UPLC-MS was performed using a Sciex TripleTOF 6600 system. Chromatographic separations were achieved using a Waters Acquity UPLC BEH C18 column (1.7 μ m, 2.1 \times 10 mm) with a flow rate of 0.4 ml/min. Data acquisition and processing were performed by Analyst and Peakview (Sciex).

Genetic ablation with miniSOG

The genetically encoded photosensitizer, miniSOG, was used to ablate specific neurons as previously described (Qi et al., 2012). Synchronized Late L1 larva animals (24 hours after egg hatching at 20°C) expressing miniSOG under specific promoters were exposed to wide-field blue light (460 nm) at an intensity of 57 mW/cm² for 30 minutes, then animals were grown in the 20 °C incubator before experiments. The ablation efficiency was measured by comparing mCherry fluorescent signal with and without blue light stimulation.

Optogenetic activation of chemosensory neurons

To prepare the plates for optogenetic activation of neurons, 1.6 mM of all-trans-retinal (ATR, 100 mM dissolved in ethanol) or ethanol (control) was mixed with OP50 *E.coli* culture and spotted on 35 mm NGM plates. Plates were allowed to dry for 24 hours before usage. Transgenic worms with channelrhodopsin variant CHIEF expressed in ASJ/ASI, AWA, AWB, or AWC chemosensory neurons were grown overnight on the NGM plates. Animals at L4 larval stages received 100 ms pulse stimulation of blue light (460 nm wavelength, 2.4 mW/mm² power) for 10 minutes (5 times) until the animals entered the adult stage.

Fluorescent microscopy imaging

For quantitative analysis of fluorescence intensities and densities, images were captured using a 100x (NA=1.4) objective on an Olympus microscope (BX53). Young adult worms were immobilized with 30 $\mu\text{g}/\mu\text{l}$ 2,3-Butanedione monoxime. The maximum intensity of dorsal cord projections of Z-series stacks was obtained by Metamorph software (Molecular Devices). Line scans were analyzed in Igor Pro (WaveMetrics) using a custom script (Dittman and Kaplan, 2006). The mean fluorescence intensities of reference FluoSphere microspheres (0.5 μm , ThermoFisher Scientific) were measured during each experiment controlled for changes in illumination intensities. To assess the synaptic accumulation of fluorescent proteins, we used the calculation of $\Delta F/F$ as $(F_{\text{puncta}} - F_{\text{axon}})/F_{\text{axon}}$. And we also counted the density of fluorescent puncta.

Electrophysiology

Electrophysiology was conducted on dissected *C. elegans* as previously described (Hu et al., 2012). Worms were superfused in an extracellular solution containing 127 mM NaCl, 5 mM KCl, 26 mM NaHCO_3 , 1.25 mM NaH_2PO_4 , 20 mM glucose, 1 mM CaCl_2 , and 4 mM MgCl_2 , bubbled with 5% CO_2 , 95% O_2 at 22 $^{\circ}\text{C}$. Whole-cell recordings were carried out at -60 mV for mEPSCs, and 0 mV for mIPSCs. The internal solution contained 105 mM $\text{CH}_3\text{O}_3\text{SCs}$, 10 mM CsCl, 15 mM CsF, 4 mM MgCl_2 , 5 mM EGTA, 0.25 mM CaCl_2 , 10 mM HEPES, and 4 mM Na_2ATP . The solution was adjusted to pH 7.2 using CsOH.

Statistics

All data were reported as mean \pm SEM (standard error of the mean). Statistical analyses were performed using GraphPad Prism (version 8). We calculated p values by two-way ANOVA (Figure 1B, 1D, 2D-F, Figure 2—figure supplement 1A-E, Figure 2—figure supplement 2, Figure 2—figure supplement 4, Figure 4—figure supplement 2A-G, Figure 4—figure supplement 3A-C), two-way ANOVA with post-hoc Sidak multiple comparisons (Figure 2B-C, 2G, 3B-C, 3F-G, 4C, 4E, 4I-J, Figure 3—figure supplement 1A-B), one-way ANOVA with post-hoc Dunnett multiple comparisons (Figure 2H-I, 3E, 4D, 7B-D, Figure 3—

figure supplement 2A-C) and unpaired Student's t-test (Figure 1F-G, 1I-J, 1L-M, 4H, 5A-E, 6D-E, Figure 1—figure supplement 1B, Figure 2—figure supplement 3A and C, Figure 6—figure supplement 1A-B). In all figures, p values are denoted as * < 0.05, ** < 0.01, *** < 0.001.

FIGURE LEGENDS:

Figure 1 The male excretome increases cholinergic synaptic transmission at hermaphrodite NMJ. (A) Schematic illustration of *C. elegans* reproduction. Hermaphrodites with two X chromosomes generate all hermaphrodite progeny via self-fertilization. While hermaphrodites are crossed with males that have a single X chromosome, an equal ratio of hermaphrodite and male offspring are generated. (B) Time course analysis of 1.4 mM aldicarb-induced paralysis in hermaphrodites generated from hermaphrodite self-fertilization (black, Self-fertilization) and hermaphrodite-male crossing (orange, Crossed). (C) Schematic illustration of conditioned medium preparation. 30,000 young-adult wild type (WT) and *him-5* mutant worms were collected and incubated in 1 ml ddH₂O for 3 hours. Metabolites secreted by hermaphrodites and males were collected and used to make hermaphrodite-conditioned (Herm-cond) and male-conditioned (Male-cond) medium. (D) Time course analysis of Aldicarb-induced paralysis in hermaphrodites cultured in hermaphrodite-conditioned medium (black, Herm-cond) and male-conditioned medium (orange, Male-cond). (E) Schematic illustration showing calcium current recording at the *C. elegans* NMJ. Chrimson driven by the *acr-5* promoter was expressed specifically in cholinergic motor neurons, and GCaMP3 under the *myo-3* promoter was expressed in the body-wall muscle. (F-G) Chrimson-evoked calcium transients in body-wall muscle were analyzed using GCaMP3 as a calcium indicator. For adult hermaphrodites cultured in hermaphrodite-conditioned medium (black, Herm-cond) or male-conditioned medium (orange, Male-cond), the averaged responses (F) and the averaged and individual relative increase in GCaMP3 fluorescence intensity $\Delta F/F$ (G) are shown. The grey shadings in F indicate the SEM of GCaMP3 responses. The dashed line indicates when the illumination with nominal wavelength at 640 nm for Chrimson activation

was applied. (H–J) Endogenous acetylcholine transmission was assessed by recording mEPSCs from body muscles of wild type adult hermaphrodites cultured in hermaphrodite-conditioned or male-conditioned medium. Representative mEPSC traces (H), the mean mEPSC rates (I), and the mean mEPSC amplitudes (J) are shown. (K–M) Endogenous GABA transmission was assessed by recording mIPSCs from body muscles of wild type adult hermaphrodites cultured in hermaphrodite-conditioned or male-conditioned medium. Representative mIPSC traces (K), the mean mIPSC rate (L), and the mean mIPSC amplitude (M) are shown. The data for individual animal analyzed are indicated. In B, D, F–G, I–J, L–M, * $p < 0.05$, *** $p < 0.001$, ns not significant, two-way ANOVA comparing all of the time points for B and D, unpaired Student's t-test for F–G, I–J, and L–M.

Figure 2 The male excretome modulates the hermaphrodite NMJ synaptic transmission in a developmental-stage-dependent manner. (A) Schematic illustration of the life cycles of *C. elegans* and the time when the hermaphrodite-conditioned medium (dashed black lines) or male-conditioned medium (solid orange lines) was applied. (B) The percentage of animals paralyzed on 1.4 mM aldicarb at 70 minutes were plotted for hermaphrodites cultured in male-conditioned medium (orange) starting from the egg stage, L1 stage, L2–L3 stage, and mid-L4 stage. Hermaphrodites cultured in hermaphrodite-conditioned medium (black) served as controls. (C) The percentage of animals paralyzed on 1.4 mM aldicarb at 70 minutes were plotted for hermaphrodites cultured in male-conditioned medium from the egg stage to the mid-L4 stage (L4 out) and young adult stage (Adult out); hermaphrodites cultured in hermaphrodite-conditioned medium (black) or male-conditioned medium (orange) served as controls. (D–F) Time course analysis of aldicarb-induced paralysis in hermaphrodites cultured in hermaphrodite-conditioned medium (black) and male-conditioned medium (orange) in CB4856 (D), AB3 (E), and TR389 (F) strains. (G) The percentage of animals paralyzed on 1.4 mM aldicarb at 80 minutes were plotted for N2 hermaphrodites cultured in N2 hermaphrodite (N2 herm-cond)-, N2 male (N2 male-cond)-, TR389 hermaphrodite (TR389 Herm-cond)- or TR389 male (TR389 Male-cond)-conditioned

medium. (H) Locomotion behavior analysis of single adult hermaphrodite cultured in N2 hermaphrodite (Herm-cond)-, TR389 male (TR389 male-cond)-, and N2 male (Male-cond)-conditioned medium. The averaged and individual crawling locomotion velocities were plotted. (I) Measurement of hermaphrodite mating efficiency cultured in N2 hermaphrodite-, TR389 male-, and N2 male-conditioned medium. In B-I, * $p < 0.05$, *** $p < 0.001$, ns not significant, two-way ANOVA with post-hoc Sidak multiple comparisons for B-C and G, two-way ANOVA comparing all of the time points for D-F, one-way ANOVA with post-hoc Dunnett multiple comparisons for H-I.

Figure 3 Ascarosides in the male environment modulate hermaphrodite NMJ synaptic transmission. (A) Proposed model of peroxisomal β -oxidation enzymes ACOX-1, MAOC-1, DHS-28, and DAF-22 in ascaroside side-chain biosynthesis. (B) The percentage of animals paralyzed on 1.4 mM aldicarb at 70 minutes were plotted for N2 hermaphrodites cultured in hermaphrodite (N2 herm-cond)-, male (N2 male-cond)-, *daf-22* mutants herm (*daf-22* herm-cond)- or *daf-22* mutant male (*daf-22* male-cond)-conditioned medium. (C) The percentage of animals paralyzed on 0.5 mM aldicarb at 100 minutes were plotted for *daf-22* mutant males cultured in hermaphrodite (N2 herm-cond)-, male (N2 male-cond)-, *daf-22* mutants herm (*daf-22* herm-cond)- or *daf-22* mutant male (*daf-22* male-cond)-conditioned medium. (D) Schematic illustration of excretome preparation for UPLC-MS. Around 30,000 freshly starved worms were cultured in S medium supplemented with concentrated OP50 for 7 days. The excretomes were collected by centrifugation, filtration, and lyophilized extraction, followed by UPLC-MS analysis. (E) β -hydroxylated ascaroside profiles in excretomes obtained from N2 hermaphrodites (N2 herm excretome), N2 mixed-gender animals of *him-5* mutants (N2 male excretome), and TR389 mixed-gender animals (TR389 male excretome). (F) The percentage of animals paralyzed on 1.4 mM aldicarb at 90 minutes were plotted for β -oxidation mutants (*acox-1.1*, *maoc-1*, and *dhs-28*). (G) The percentage of animals paralyzed on 1.4 mM aldicarb at 70 minutes were plotted for N2 and *dhs-28* mutant

hermaphrodites cultured in hermaphrodite-conditioned medium (Herm-cond), male-conditioned medium (Male-cond). In B-C, E-G, * $p < 0.05$, ** $p < 0.01$, *** $p < 0.001$, ns not significant, two-way ANOVA with post-hoc Sidak multiple comparisons for B-C and F-G. one-way ANOVA with post-hoc Dunnett multiple comparisons for E.

Figure 4 AWB neurons sense the modulator ascarosides. (A) The table lists all of the chemosensory neurons examined in the screen, the neuron-specific promoters used to drive miniSOG expression, and the impact of neuron ablation on sensing of modulator ascarosides. (B) Representative images showing that mCherry-labeled AWB neurons were specifically ablated by blue light-induced miniSOG activation. Scale bar, 40 μm . (C) The percentage of animals paralyzed on 1.4 mM aldicarb at 80 minutes were plotted for hermaphrodites expressing miniSOG in AWB neurons (*str-1* promoter) with and without blue-light induced ablation. Black: cultured in hermaphrodite-conditioned medium; Orange: cultured in male-conditioned medium. (D) Locomotion behavior analysis of single adult worm from AWB ablated hermaphrodites in hermaphrodite- and male-conditioned medium. The averaged crawling locomotion velocities were plotted. (E) The percentage of animals paralyzed on 1.4 mM aldicarb at 90 minutes were plotted for hermaphrodites with AWB neurons optogenetically activated during the L4 stage. The channelrhodopsin variant CHIEF was expressed in AWB chemosensory neurons driven by the *str-1* promoter. The blue light was turned on to excite AWBs in transgenic animals fed with or without ATR. (F) Top panel: snapshots of GCaMP6f fluorescent signals of an AWB neuron before, during, and after addition of male excretome. Scale bar, 10 μm . Bottom panel: the calcium trace showing the AWB neuron activated by male excretome. (G) Curves and average intensities of Ca^{2+} signals evoked by the hermaphrodite or male excretome in the soma of AWB with GCaMP6f expression. The shaded box represents the addition of the hermaphrodite or male excretome. (H) Scatter diagram and quantification of the Ca^{2+} change. Each point represents Ca^{2+} peak value from one animal. (I) The percentages of animals paralyzed on 1.4 mM

aldicarb at 80 minutes were plotted for *tax-2(p691)* mutant hermaphrodites and TAX-2 expression restored in AWB or ASJ/ASI neurons cultured in hermaphrodite- (black) and male-conditioned medium (orange). (J) The percentages of animals paralyzed on 1.4 mM aldicarb at 80 minutes were plotted for *odr-3(n1605)* mutant hermaphrodites and ODR-3 expression restored in AWB neurons cultured in hermaphrodite- (black) and male-conditioned medium (orange). In C-E, H-J, *** $p < 0.001$, ** $p < 0.01$, ns not significant, two-way ANOVA with post-hoc Sidak multiple comparisons for C, E and I-J, one-way ANOVA with post-hoc Dunnett multiple comparisons for D, unpaired Student's t-test for H.

Figure 5 Modulator ascarosides promote postsynaptic AchR synaptic localization. (A)

The puncta fluorescence intensities and densities marked by the excitatory synaptic GFP::RAB-3 (under *unc-129* promoter) in dorsal nerve cord axons were unaltered by modulator ascarosides. Representative images (top panel), mean puncta intensities and puncta density (bottom panel) are shown for hermaphrodites grown in hermaphrodite- or male-conditioned medium. (B) The puncta fluorescence intensities and densities marked by the inhibitory synaptic RFP::RAB-3 (under *unc-25* promoter) were unaltered in hermaphrodites cultured in male-conditioned medium. Representative images (top panel), mean puncta intensities and puncta density (bottom panel) are shown. (C-E) The muscle-specific ACR-16::RFP, UNC-29::RFP, and UNC-49::RFP fluorescence intensities and densities in hermaphrodites cultured in hermaphrodite- and male-conditioned medium. Representative images, mean puncta intensities and puncta density are shown separately. Scale bars, 5 μm . ** $p < 0.005$, *** $p < 0.001$, ns not significant, unpaired Student's t-test.

Figure 6 Modulator ascarosides increase the abundance of excitatory presynaptic

CaV2 calcium channels at the NMJ. (A) Schematic illustration of split GFP experimental design. Seven copies of the splitGFP 11 were inserted into the C-terminal of *unc-2* genomic loci by CRISPR-Cas9 system. The splitGFP1-10 was expressed in B-type cholinergic and

GABAergic motor neurons by *unc-129* and *unc-47* promoters. The *unc-57-mCherry* under the same promoter was separated with splitGFP1-10 by SL2, and was also used as a coexpressed presynaptic marker. (B-C) Presynaptic UNC-2::splitGFP (green) and UNC-57::mCherry (red) were co-localized in the dorsal nerve cord at both excitatory (B) and inhibitory (C) synapses. Representative images (top, scale bar, 10 μ m) and linescan curves (bottom) are shown. For linescan curves, the mCherry signals were plotted on the left Y-axis, while the splitGFP signals were plotted on the right. 1 arbitrary fluorescence intensity unit equals 100 gray value. (D-E) The puncta fluorescence intensities and densities of UNC-2::splitGFP in B-type motor neurons (D) and GABAergic motor neurons (E) of hermaphrodites cultured in hermaphrodite- or male-conditioned medium. Representative images (scale bar, 5 μ m), mean puncta intensities, and puncta densities are shown. In D and E, * $p < 0.05$, ** $p < 0.01$, ns not significant, unpaired Student's t-test.

Figure 7 CaV2 calcium channel is the synaptic target of the modulator ascarosides.

(A–C) Endogenous acetylcholine transmission was assessed by recording mEPSCs from body muscles of wild type N2 and *unc-2* mutant adult hermaphrodites cultured in hermaphrodite- or male-conditioned medium. Representative mEPSC traces (A), the mean mEPSC rates (B), and the mean mEPSC amplitudes (C) are shown. The data for wild type (N2) is the same as in Figure 1H-J. (D) Locomotion behavior analysis of the single wild type and *unc-2* mutant hermaphrodite in hermaphrodite- and male-conditioned medium. The averaged and individual locomotion velocities were plotted. In B-D, * $p < 0.05$, *** $p < 0.001$, ns not significant, one-way ANOVA with post-hoc Dunnett multiple comparisons.

Figure 1—figure supplement 1 The physiological muscle excitability is potentiated in hermaphrodites from the male-conditioned medium. (A) Averaged Chrimson-evoked calcium transients in body-wall muscle were analyzed in hermaphrodites cultured in hermaphrodite-conditioned medium (black) or male-conditioned medium (orange). The

averaged responses (A) and the endogenous GCaMP3 fluorescence intensity (B) were shown. The gray and orange shadings in A indicate SEM of GCaMP3 responses. The numbers of animals are indicated inside the bars. In B, * $p < 0.05$, unpaired Student's t-test.

Figure 2—figure supplement 1 The male environment modulates the hermaphrodite NMJ synaptic transmission in a developmental-stage-dependent manner. (A-D) Time course analysis of aldicarb-induced paralysis in hermaphrodites cultured in male-conditioned medium (orange) starting from egg stage (A), L1 (B), L2-L3 stage (C), and mid-L4 stage (D). Hermaphrodites cultured in hermaphrodite-conditioned medium (black) served as controls. (E) Time course analysis of aldicarb-induced paralysis in hermaphrodites cultured in male-conditioned medium from the egg stage to the L4 (pink) and young adult stage (dark red), hermaphrodites cultured in hermaphrodite-conditioned medium (black), and male-conditioned medium (orange). *** $p < 0.001$, ns not significant, two-way ANOVA comparing all of the time points.

Figure 2—figure supplement 2 TR389 hermaphrodites can be modulated by the modulator ascarosides. Time course analysis of aldicarb-induced paralysis in TR389 hermaphrodite grown under N2 hermaphrodite (black, N2 herm-cond)- or N2 male-conditioned (orange, N2 male-cond) medium. *** $p < 0.001$, ns not significant, two-way ANOVA comparing all of the time points.

Figure 2—figure supplement 3 The male excretome does not change hermaphrodite body-bend curvature. (A) Scatter plot showing the body-bend curvature in hermaphrodites (black) and males (red). (B) Color plot showing the waves of curvature propagating along the body of representative hermaphrodite (Herm, top) and male (Male, bottom). (C) Scatter plot showing the body-bend curvature in hermaphrodites from hermaphrodite- (black) and male-conditioned (orange) medium. (D) Color plot showing the waves of curvature propagating along the body of representative hermaphrodite from hermaphrodite- (top) and male-

conditioned (bottom) medium. In A and C, *** $p < 0.001$, ns not significant, unpaired Student's t-test.

Figure 2—figure supplement 4 The male excretome does not modulate hermaphrodite brood size. Time course analysis of the average number of eggs laid by hermaphrodites from hermaphrodite- and male-conditioned medium. ns not significant, two-way ANOVA comparing all of the time points.

Figure 3—figure supplement 1 The male environment cannot modulate NMJ synaptic transmission in males. The percentage of animals paralyzed on 0.5mM (A) or 1.4 mM (B) aldicarb at 90 minutes were plotted for wild type males (A) and *daf-22* mutant hermaphrodites (B) cultured in N2- and *daf-22* mutant-conditioned medium. *** $p < 0.001$, ns not significant, two-way ANOVA with post-hoc Sidak multiple comparisons.

Figure 3—figure supplement 2 UPLC-MS analysis of excretome from animal cultures. (A) The relative abundance of *ascr#10* in excretomes obtained from N2 hermaphrodites (N2 herm excre), N2 mixed-gender animals of *him-5* mutants (N2 male excre), and TR389 mixed-gender animals (TR389 male excre). (B) Ascaroside profiles in excretomes obtained from N2 mixed-gender animals of *him-5* mutants (N2 male excretome) and *daf-22* mixed-gender animals (*daf-22* male excretome) showed that long-chain ascarosides were accumulated in *daf-22* mutant cultures. (C) Saturated ascaroside profiles in excretomes obtained from N2 hermaphrodites (N2 excretome), N2 mixed-gender animals of *him-5* mutants (N2 male excretome), and TR389 mixed-gender animals (TR389 male excretome). * $p < 0.05$, ** $p < 0.01$, one-way ANOVA with post-hoc Dunnett multiple comparisons.

Figure 4—figure supplement 1 Genetic ablation efficiency by miniSOG. (A) Schematic illustration of blue light stimulation pattern. (B) Representative images of multiple

chemosensory neurons expressing miniSOG and mCherry (*flp-21* promoter) before (no blue light) and after (weak and strong) blue light stimulation (scale bar, 5 μ m). (C) Ablation efficiency was calculated after 15, 30, and 50 minutes of blue light stimulation. Weak and strong labels indicated ablation efficiencies by examining mCherry fluorescent signals in chemosensory neurons. The numbers of animals analyzed were indicated for each condition.

Figure 4—figure supplement 2 ASE, AWC, AWA, ASH, ASI, ADF, ASG, ASK, ADL, and ASJ chemosensory neurons are dispensable for sensing modulator ascarodites. Time course analysis of aldicarb-induced paralysis in hermaphrodites with ablated ASE/AWC (*ceh-36* promoter, A), AWA (*odr-10* promoter, B), ASH/ADF/ADL (*srb-6* promoter, C), ASI (*gpa-4* promoter, D), ASG (*gcy-15* promoter, E), ASK (*sra-7* promoter, F) and ASJ/ASI (*daf-28* promoter, G) grown in hermaphrodite-conditioned medium (black) or male-conditioned medium (orange). ** $p < 0.01$, *** $p < 0.001$, two-way ANOVA comparing all of the time points.

Figure 4—figure supplement 3 Activation of other sensory neurons does not change aldicarb sensitivity in hermaphrodites. (A-C) Time course analysis of aldicarb-induced paralysis in hermaphrodites with ASJ/ASI (A), AWA (B), or AWC (C) optogenetically activated during the L3-L4 stage. The channelrhodopsin variant CHIEF was expressed in ASJ/ASI, AWA or AWC chemosensory neurons driven by the neuron-specific *daf-28*, *odr-10* and *str-2* promoters. The blue light was turned on (orange) or off (black) in the presence of ATR. *** $p < 0.001$, ns not significant, two-way ANOVA comparing all of the time points.

Figure 6—figure supplement 1 Excitatory and inhibitory synapse structures are not affected by the modulator ascarosides. (A) The puncta fluorescence intensities and densities marked by the excitatory synaptic UNC-57::mCherry (under *unc-129* promoter) in dorsal nerve cord axons were unaltered by modulator ascarosides. Representative images

1083 (top panel), mean puncta intensities and puncta density (bottom panel) are shown for
1084 hermaphrodites grown in hermaphrodite- or male-conditioned medium. (B) The puncta
1085 fluorescence intensities and densities marked by the inhibitory synaptic UNC-57::mCherry
1086 (under *unc-47* promoter) were unaltered in hermaphrodites cultured in male-conditioned
1087 medium. Representative images (top panel), mean puncta intensities and puncta density
1088 (bottom panel) are shown. ns not significant, unpaired Student's t-test.

REFERENCES:

- 1089 Alcazar, R.M., Lin, R.L., and Fire, A.Z. (2008). Transmission Dynamics of Heritable Silencing
1090 Induced by Double-Stranded RNA in *Caenorhabditis elegans*. *Genetics* 180, 1275-1288.
- 1091 Aprison, E.Z., and Ruvinsky, I. (2017). Counteracting Ascarosides Act through Distinct
1092 Neurons to Determine the Sexual Identity of *C. elegans* Pheromones. *Curr Biol* 27, 2589-
1093 2599.
- 1094 Aprison, E.Z., and Ruvinsky, I. (2019a). Coordinated Behavioral and Physiological
1095 Responses to a Social Signal Are Regulated by a Shared Neuronal Circuit. *Curr Biol* 29,
1096 4108-4115.
- 1097 Aprison, E.Z., and Ruvinsky, I. (2019b). Dynamic Regulation of Adult-Specific Functions of
1098 the Nervous System by Signaling from the Reproductive System. *Curr Biol* 29, 4116-4123.
- 1099 Banerjee, N., and Hallem, E. (2018). Sexual Dimorphisms: How Sex-Shared Neurons
1100 Generate Sex-Specific Behaviors. *Curr Biol* 28, R254-R256.
- 1101 Bargmann, C.I. (2006). Chemosensation in *C. elegans*. *WormBook*, 1-29.
- 1102 Bayer, E.A., and Hobert, O. (2018). Past experience shapes sexually dimorphic neuronal
1103 wiring through monoaminergic signalling. *Nature* 561, 117-121.
- 1104 Borcel, E., Palczynska, M., Krzisch, M., Dimitrov, M., Ulrich, G., Toni, N., and Fraering, P.C.
1105 (2016). Shedding of neurexin 3 beta ectodomain by ADAM10 releases a soluble fragment
1106 that affects the development of newborn neurons. *Sci Rep-Uk* 6.

1107 Butcher, R.A., Fujita, M., Schroeder, F.C., and Clardy, J. (2007). Small-molecule
 1108 pheromones that control dauer development in *Caenorhabditis elegans*. *Nat Chem Biol* 3,
 1109 420-422.

1110 Butcher, R.A., Ragains, J.R., Li, W.Q., Ruvkun, G., Clardy, J., and Mak, H.Y. (2009).
 1111 Biosynthesis of the *Caenorhabditis elegans* dauer pheromone. *P Natl Acad Sci USA* 106,
 1112 1875-1879.

1113 Cabantous, S., Terwilliger, T.C., and Waldo, G.S. (2005). Protein tagging and detection with
 1114 engineered self-assembling fragments of green fluorescent protein. *Nature Biotechnology* 23,
 1115 102-107.

1116 Chao, H.T., Zoghbi, H.Y., and Rosenmund, C. (2007). MeCP2 controls excitatory synaptic
 1117 strength by regulating glutamatergic synapse number. *Neuron* 56, 58-65.

1118 Chen, P., and Hong, W.Z. (2018). Neural Circuit Mechanisms of Social Behavior. *Neuron* 98,
 1119 16-30.

1120 Chen, Q., Deister, C.A., Gao, X., Guo, B.L., Lynn-Jones, T., Chen, N.Y., Wells, M.F., Liu,
 1121 R.P., Goard, M.J., Dimidschstein, J., *et al.* (2020). Dysfunction of cortical GABAergic
 1122 neurons leads to sensory hyper-reactivity in a Shank3 mouse model of ASD. *Nat Neurosci*.

1123 Colavita, A., Krishna, S., Zheng, H., Padgett, R.W., and Culotti, J.G. (1998). Pioneer axon
 1124 guidance by UNC-129, a *C-elegans* TGF-beta. *Science* 281, 706-709.

1125 Cook, S.J., Jarrell, T.A., Brittin, C.A., Wang, Y., Bloniarz, A.E., Yakovlev, M.A., Nguyen,
 1126 K.C.Q., Tang, L.T.H., Bayer, E.A., Duerr, J.S., *et al.* (2019). Whole-animal connectomes of
 1127 both *Caenorhabditis elegans* sexes. *Nature* 571, 63-71.

1128 Dittman, J.S., and Kaplan, J.M. (2006). Factors regulating the abundance and localization of
 1129 synaptobrevin in the plasma membrane. *P Natl Acad Sci USA* 103, 11399-11404.

1130 Doan, R.N., Bae, B.I., Cubelos, B., Chang, C., Hossain, A.A., Al-Saad, S., Mukaddes, N.M.,
 1131 Oner, O., Al-Saffar, M., Balkhy, S., *et al.* (2016). Mutations in Human Accelerated Regions
 1132 Disrupt Cognition and Social Behavior. *Cell* 167, 341-354.

1133 Doan, R.N., Lim, E.T., De Rubeis, S., Betancur, C., Cutler, D.J., Chiocchetti, A.G., Overman,
 1134 L.M., Soucy, A., Goetze, S., Freitag, C.M., *et al.* (2019). Recessive gene disruptions in
 1135 autism spectrum disorder. *Nat Genet* 51, 1092-1098.
 1136 Dolphin, A.C., and Lee, A. (2020). Presynaptic calcium channels: specialized control of
 1137 synaptic neurotransmitter release. *Nature Reviews Neuroscience* 21, 213-229.
 1138 Dong, C.F., Dolke, F., and von Reuss, S.H. (2016). Selective MS screening reveals a sex
 1139 pheromone in *Caenorhabditis briggsae* and species-specificity in indole ascaroside
 1140 signalling. *Org Biomol Chem* 14, 7217-7225.
 1141 Edison, A.S. (2009). *Caenorhabditis elegans* pheromones regulate multiple complex
 1142 behaviors. *Curr Opin Neurobiol* 19, 378-388.
 1143 Emmons, S.W. (2018). Neural Circuits of Sexual Behavior in *Caenorhabditis elegans*. *Annu*
 1144 *Rev Neurosci* 41, 349-369.
 1145 Fagan, K.A., Luo, J.T., Lagoy, R.C., Schroeder, F.C., Albrecht, D.R., and Portman, D.S.
 1146 (2018). A Single-Neuron Chemosensory Switch Determines the Valence of a Sexually
 1147 Dimorphic Sensory Behavior. *Curr Biol* 28, 902-914.
 1148 Frokjaer-Jensen, C., Davis, M.W., Sarov, M., Taylor, J., Flibotte, S., LaBella, M.,
 1149 Pozniakovsky, A., Moerman, D.G., and Jorgensen, E.M. (2014). Random and targeted
 1150 transgene insertion in *Caenorhabditis elegans* using a modified Mos1 transposon. *Nature*
 1151 *Methods* 11, 529-534.
 1152 Garcia, L.R., and Portman, D.S. (2016). Neural circuits for sexually dimorphic and sexually
 1153 divergent behaviors in *Caenorhabditis elegans*. *Curr Opin Neurobiol* 38, 46-52.
 1154 Garrison, J.L. (2012). Oxytocin/vasopressin-related peptides have an ancient role in
 1155 reproductive behavior (vol 338, pg 540, 2012). *Science* 338, 1029-1029.
 1156 Geisheker, M.R., Heymann, G., Wang, T.Y., Coe, B.P., Turner, T.N., Stessman, H.A.F.,
 1157 Hoekzema, K., Kvarnung, M., Shaw, M., Friend, K., *et al.* (2017). Hotspots of missense
 1158 mutation identify neurodevelopmental disorder genes and functional domains. *Nat Neurosci*
 1159 20, 1043-1051.

1160 Greene, J.S., Brown, M., Dobosiewicz, M., Ishida, I.G., Macosko, E.Z., Zhang, X.X., Butcher,
 1161 R.A., Cline, D.J., McGrath, P.T., and Bargmann, C.I. (2016). Balancing selection shapes
 1162 density-dependent foraging behaviour. *Nature* 539, 254-258.
 1163 Hart, M.P., and Hobert, O. (2018). Neurexin controls plasticity of a mature, sexually
 1164 dimorphic neuron. *Nature* 553, 165-170.
 1165 Hata, Y., Slaughter, C.A., and Sudhof, T.C. (1993). Synaptic Vesicle Fusion Complex
 1166 Contains Unc-18 Homolog Bound to Syntaxin. *Nature* 366, 347-351.
 1167 Hu, Z.T., Hom, S., Kudze, T., Tong, X.J., Choi, S., Aramuni, G., Zhang, W.Q., and Kaplan,
 1168 J.M. (2012). Neurexin and Neuroligin Mediate Retrograde Synaptic Inhibition in *C. elegans*.
 1169 *Science* 337, 980-984.
 1170 Iossifov, I., Ronemus, M., Levy, D., Wang, Z.H., Hakker, I., Rosenbaum, J., Yamrom, B.,
 1171 Lee, Y.H., Narzisi, G., Leotta, A., *et al.* (2012). De Novo Gene Disruptions in Children on the
 1172 Autistic Spectrum. *Neuron* 74, 285-299.
 1173 Isogai, Y., Wu, Z., Love, M.I., Ahn, M.H.Y., Bambah-Mukku, D., Hua, V., Farrell, K., and
 1174 Dulac, C. (2018). Multisensory Logic of Infant-Directed Aggression by Males. *Cell* 175, 1827-
 1175 1841.
 1176 Izrayelit, Y., Srinivasan, J., Campbell, S.L., Jo, Y., von Reuss, S.H., Genoff, M.C., Sternberg,
 1177 P.W., and Schroeder, F.C. (2012). Targeted metabolomics reveals a male pheromone and
 1178 sex-specific ascaroside biosynthesis in *Caenorhabditis elegans*. *ACS Chem Biol* 7, 1321-
 1179 1325.
 1180 Jin, Y., Jorgensen, E., Hartwig, E., and Horvitz, H.R. (1999). The *Caenorhabditis elegans*
 1181 gene *unc-25* encodes glutamic acid decarboxylase and is required for synaptic transmission
 1182 but not synaptic development. *J Neurosci* 19, 539-548.
 1183 Judson, M.C., Wallace, M.L., Sidorov, M.S., Burette, A.C., Gu, B., van Woerden, G.M., King,
 1184 I.F., Han, J.E., Zylka, M.J., Elgersma, Y., *et al.* (2016). GABAergic Neuron-Specific Loss of
 1185 Ube3a Causes Angelman Syndrome-Like EEG Abnormalities and Enhances Seizure
 1186 Susceptibility. *Neuron* 90, 56-69.

1187 Kamiyama, D., Sekine, S., Barsi-Rhyne, B., Hu, J., Chen, B.H., Gilbert, L.A., Ishikawa, H.,
 1188 Leonetti, M.D., Marshall, W.F., Weissman, J.S., *et al.* (2016). Versatile protein tagging in
 1189 cells with split fluorescent protein. *Nat Commun* 7.
 1190 Klapoetke, N.C., Murata, Y., Kim, S.S., Pulver, S.R., Birdsey-Benson, A., Cho, Y.K.,
 1191 Morimoto, T.K., Chuong, A.S., Carpenter, E.J., Tian, Z.J., *et al.* (2014). Independent optical
 1192 excitation of distinct neural populations. *Nature Methods* 11, 338-346.
 1193 Kurshan, P.T., Merrill, S.A., Dong, Y.M., Ding, C., Hammarlund, M., Bai, J.H., Jorgensen,
 1194 E.M., and Shen, K. (2018). gamma-Neurexin and Frizzled Mediate Parallel Synapse
 1195 Assembly Pathways Antagonized by Receptor Endocytosis. *Neuron* 100, 150-166.
 1196 Lee, C., Kang, E.Y., Ganda, M.J., Eskin, E., and Geschwind, D.H. (2019). Profiling allele-
 1197 specific gene expression in brains from individuals with autism spectrum disorder reveals
 1198 preferential minor allele usage. *Nat Neurosci* 22, 1521-1532.
 1199 Lee, J., Chung, C., Ha, S., Lee, D., Kim, D.Y., Kim, H., and Kim, E. (2015). Shank3-mutant
 1200 mice lacking exon 9 show altered excitation/inhibition balance, enhanced rearing, and spatial
 1201 memory deficit. *Front Cell Neurosci* 9.
 1202 Levinson, J.N., and El-Husseini, A. (2005). Building excitatory and inhibitory synapses:
 1203 Balancing neuroligin partnerships. *Neuron* 48, 171-174.
 1204 Li, Q., and Liberles, S.D. (2015). Aversion and Attraction through Olfaction. *Curr Biol* 25,
 1205 R120-R129.
 1206 Liberles, S.D. (2014). Mammalian pheromones. *Annu Rev Physiol* 76, 151-175.
 1207 Liu, H., Qin, L., Li, R., Zhang, C., Al-Sheikh, U., and Wu, Z. (2019). Reciprocal modulation of
 1208 5-HT and octopamine regulates pumping via feedforward and feedback circuits in *C.*
 1209 *elegans*. *Proc Natl Acad Sci U S A* 116, 10598.
 1210 Liu, H.W., Li, L., Wang, W., Gong, J.H., Yang, X.F., and Hu, Z.T. (2018). Spontaneous
 1211 Vesicle Fusion Is Differentially Regulated at Cholinergic and GABAergic Synapses. *Cell Rep*
 1212 22, 2334-2345.
 1213 Ludewig, A.H., Artyukhin, A.B., Aprison, E.Z., Rodrigues, P.R., Pulido, D.C., Burkhardt, R.N.,
 1214 Panda, O., Zhang, Y.K., Gudibanda, P., Ruvinsky, I., *et al.* (2019). An excreted small

1215 molecule promotes *C. elegans* reproductive development and aging. *Nat Chem Biol* 15, 838-
1216 845.

1217 Ludewig, A.H., and Schroeder, F.C. (2013). Ascaroside signaling in *C. elegans*. *WormBook* :
1218 the online review of *C. elegans* biology, 1-22.

1219 Luo, F.J., Sclip, A., Jiang, M., and Sudhof, T.C. (2020). Neurexins cluster Ca²⁺ channels
1220 within the presynaptic active zone. *Embo Journal* 39.

1221 Mahoney, T.R., Luo, S., and Nonet, M.L. (2006). Analysis of synaptic transmission in
1222 *Caenorhabditis elegans* using an aldicarb-sensitivity assay. *Nat Protoc* 1, 1772-1777.

1223 Maro, G.S., Gao, S.B., Olechwie, A.M., Hung, W.L., Liu, M., Ozkan, E., Zhen, M., and Shen,
1224 K. (2015). MADD-4/Punctin and Neurexin Organize *C. elegans* GABAergic Postsynapses
1225 through Neuroligin. *Neuron* 86, 1420-1432.

1226 Maures, T.J., Booth, L.N., Benayoun, B.A., Izrayelit, Y., Schroeder, F.C., and Brunet, A.
1227 (2014). Males Shorten the Life Span of *C. elegans* Hermaphrodites via Secreted
1228 Compounds. *Science* 343, 541-544.

1229 Miyazaki, T., Takase, K., Nakajima, W., Tada, H., Ohya, D., Sano, A., Goto, T., Hirase, H.,
1230 Malinow, R., and Takahashi, T. (2012). Disrupted cortical function underlies behavior
1231 dysfunction due to social isolation. *J Clin Invest* 122, 2690-2701.

1232 Morrow, E.M., Yoo, S.Y., Flavell, S.W., Kim, T.K., Lin, Y.X., Hill, R.S., Mukaddes, N.M.,
1233 Balkhy, S., Gascon, G., Hashmi, A., *et al.* (2008). Identifying autism loci and genes by
1234 tracing recent shared ancestry. *Science* 321, 218-223.

1235 Mowrey, W.R., Bennett, J.R., and Portman, D.S. (2014). Distributed Effects of Biological Sex
1236 Define Sex-Typical Motor Behavior in *Caenorhabditis elegans*. *Journal of Neuroscience* 34,
1237 1579-1591.

1238 Nanou, E., and Catterall, W.A. (2018). Calcium Channels, Synaptic Plasticity, and
1239 Neuropsychiatric Disease. *Neuron* 98, 466-481.

1240 Narayan, A., Venkatachalam, V., Durak, O., Reilly, D.K., Bose, N., Schroeder, F.C., Samuel,
1241 A.D.T., Srinivasan, J., and Sternberg, P.W. (2016). Contrasting responses within a single

1242 neuron class enable sex-specific attraction in *Caenorhabditis elegans*. *P Natl Acad Sci USA*
 1243 113, E1392-E1401.

1244 Neale, B.M., Kou, Y., Liu, L., Ma'ayan, A., Samocha, K.E., Sabo, A., Lin, C.F., Stevens, C.,
 1245 Wang, L.S., Makarov, V., *et al.* (2012). Patterns and rates of exonic de novo mutations in
 1246 autism spectrum disorders. *Nature* 485, 242-245.

1247 Ogawa, H., Harada, S., Sassa, T., Yamamoto, H., and Hosono, R. (1998). Functional
 1248 properties of the *unc-64* gene encoding a *Caenorhabditis elegans* syntaxin. *Journal of*
 1249 *Biological Chemistry* 273, 2192-2198.

1250 Olmos-Serrano, J.L., Paluszkievicz, S.M., Martin, B.S., Kaufmann, W.E., Corbin, J.G., and
 1251 Huntsman, M.M. (2010). Defective GABAergic Neurotransmission and Pharmacological
 1252 Rescue of Neuronal Hyperexcitability in the Amygdala in a Mouse Model of Fragile X
 1253 Syndrome. *Journal of Neuroscience* 30, 9929-9938.

1254 Orefice, L.L., Mosko, J.R., Morency, D.T., Wells, M.F., Tasnim, A., Mozeika, S.M., Ye, M.C.,
 1255 Chirila, A.M., Emanuel, A.J., Rankin, G., *et al.* (2019). Targeting Peripheral Somatosensory
 1256 Neurons to Improve Tactile-Related Phenotypes in ASD Models. *Cell* 178, 867-886.

1257 Pevsner, J., Hsu, S.C., Braun, J.E.A., Calakos, N., Ting, A.E., Bennett, M.K., and Scheller,
 1258 R.H. (1994). Specificity and Regulation of a Synaptic Vesicle Docking Complex. *Neuron* 13,
 1259 353-361.

1260 Philbrook, A., Ramachandran, S., Lambert, C.M., Oliver, D., Florman, J., Alkema, M.J.,
 1261 Lemons, M., and Francis, M.M. (2018). Neurexin directs partner-specific synaptic
 1262 connectivity in *C-elegans*. *Elife* 7.

1263 Pouloupoulos, A., Aramuni, G., Meyer, G., Soykan, T., Hoon, M., Papadopoulos, T., Zhang,
 1264 M.Y., Paarmann, I., Fuchs, C., Harvey, K., *et al.* (2009). Neuroligin 2 Drives Postsynaptic
 1265 Assembly at Perisomatic Inhibitory Synapses through Gephyrin and Collybistin. *Neuron* 63,
 1266 628-642.

1267 Qi, Y.B., Garren, E.J., Shu, X., Tsien, R.Y., and Jin, Y. (2012). Photo-inducible cell ablation
 1268 in *Caenorhabditis elegans* using the genetically encoded singlet oxygen generating protein
 1269 miniSOG. *Proc Natl Acad Sci U S A* 109, 7499-7504.

1270 Rechavi, O., Minevich, G., and Hobert, O. (2011). Transgenerational Inheritance of an
 1271 Acquired Small RNA-Based Antiviral Response in *C. elegans*. *Cell* 147, 1248-1256.
 1272 Richmond, J.E., Davis, W.S., and Jorgensen, E.M. (1999). UNC-13 is required for synaptic
 1273 vesicle fusion in *C-elegans*. *Nat Neurosci* 2, 959-964.
 1274 Richmond, J.E., and Jorgensen, E.M. (1999). One GABA and two acetylcholine receptors
 1275 function at the *C-elegans* neuromuscular junction. *Nat Neurosci* 2, 791-797.
 1276 Rizo, J., and Sudhof, T.C. (2012). The Membrane Fusion Enigma: SNAREs, Sec1/Munc18
 1277 Proteins, and Their Accomplices-Guilty as Charged? *Annu Rev Cell Dev Bi* 28, 279-308.
 1278 Shi, C., and Murphy, C.T. (2014). Mating Induces Shrinking and Death in *Caenorhabditis*
 1279 Mothers. *Science* 343, 536-540.
 1280 Shi, C., Runnels, A.M., and Murphy, C.T. (2017). Mating and male pheromone kill
 1281 *Caenorhabditis* males through distinct mechanisms. *Elife* 6.
 1282 Srinivasan, J., Kaplan, F., Ajredini, R., Zachariah, C., Alborn, H.T., Teal, P.E., Malik, R.U.,
 1283 Edison, A.S., Sternberg, P.W., and Schroeder, F.C. (2008). A blend of small molecules
 1284 regulates both mating and development in *Caenorhabditis elegans*. *Nature* 454, 1115-1118.
 1285 Srinivasan, J., von Reuss, S.H., Bose, N., Zaslaver, A., Mahanti, P., Ho, M.C., O'Doherty,
 1286 O.G., Edison, A.S., Sternberg, P.W., and Schroeder, F.C. (2012). A Modular Library of Small
 1287 Molecule Signals Regulates Social Behaviors in *Caenorhabditis elegans*. *Plos Biol* 10.
 1288 Sudhof, T.C. (2008). Neuroligins and neurexins link synaptic function to cognitive disease.
 1289 *Nature* 455, 903-911.
 1290 Tchenio, A., Lecca, S., Valentinova, K., and Mameli, M. (2017). Limiting habenular
 1291 hyperactivity ameliorates maternal separation-driven depressive-like symptoms. *Nat*
 1292 *Commun* 8.
 1293 Tian, L., Hires, S.A., Mao, T., Huber, D., Chiappe, M.E., Chalasani, S.H., Petreanu, L.,
 1294 Akerboom, J., McKinney, S.A., Schreiter, E.R., *et al.* (2009). Imaging neural activity in
 1295 worms, flies and mice with improved GCaMP calcium indicators. *Nature Methods* 6, 875-881.
 1296 Tong, X.J., Hu, Z.T., Liu, Y., Anderson, D., and Kaplan, J.M. (2015). A network of autism
 1297 linked genes stabilizes two pools of synaptic GABA(A) receptors. *Elife* 4.

1298 Tong, X.J., Lopez-Soto, E.J., Li, L., Liu, H.W., Nedelcu, D., Lipscombe, D., Hu, Z.T., and
 1299 Kaplan, J.M. (2017). Retrograde Synaptic Inhibition Is Mediated by alpha-Neurexin Binding
 1300 to the alpha 2 delta Subunits of N-Type Calcium Channels. *Neuron* 95, 326-340.
 1301 Tu, H.J., Pinan-Lucarre, B., Ji, T.T., Jospin, M., and Bessereau, J.L. (2015). C. elegans
 1302 Punctin Clusters GABA(A) Receptors via Neuroligin Binding and UNC-40/DCC Recruitment.
 1303 *Neuron* 86, 1407-1419.
 1304 Vashlishan, A.B., Madison, J.M., Dybbs, M., Bai, J., Sieburth, D., Ch'ng, Q., Tavazoie, M.,
 1305 and Kaplan, J.M. (2008). An RNAi screen identifies genes that regulate GABA synapses.
 1306 *Neuron* 58, 346-361.
 1307 von Reuss, S.H., Bose, N., Srinivasan, J., Yim, J.J., Judkins, J.C., Sternberg, P.W., and
 1308 Schroeder, F.C. (2012). Comparative Metabolomics Reveals Biogenesis of Ascarosides, a
 1309 Modular Library of Small-Molecule Signals in C. elegans. *J Am Chem Soc* 134, 1817-1824.
 1310 Wallace, M.L., Burette, A.C., Weinberg, R.J., and Philpot, B.D. (2012). Maternal Loss of
 1311 Ube3a Produces an Excitatory/Inhibitory Imbalance through Neuron Type-Specific Synaptic
 1312 Defects. *Neuron* 74, 793-800.
 1313 Wan, X., Zhou, Y., Chan, C.M., Yang, H.N., Yeung, C., and Chow, K.L. (2019). SRD-1 in
 1314 AWA neurons is the receptor for female volatile sex pheromones in C. elegans males. *Embo*
 1315 *Reports* 20.
 1316 Whitaker, L.R., Degoulet, M., and Morikawa, H. (2013). Social Deprivation Enhances VTA
 1317 Synaptic Plasticity and Drug-Induced Contextual Learning. *Neuron* 77, 335-345.
 1318 Wu, T., Duan, F., Yang, W., Liu, H., Caballero, A., Fernandes de Abreu, D.A., Dar, A.R.,
 1319 Alcedo, J., Ch'ng, Q., Butcher, R.A., *et al.* (2019). Pheromones Modulate Learning by
 1320 Regulating the Balanced Signals of Two Insulin-like Peptides. *Neuron* 104, 1095-1109.
 1321 Yin, J.A., Gao, G., Liu, X.J., Hao, Z.Q., Li, K., Kang, X.L., Li, H., Shan, Y.H., Hu, W.L., Li,
 1322 H.P., *et al.* (2017). Genetic variation in glia-neuron signalling modulates ageing rate. *Nature*
 1323 551, 198-203.
 1324 Yuen, R.K.C., Merico, D., Bookman, M., Howe, J.L., Thiruvahindrapuram, B., Patel, R.V.,
 1325 Whitney, J., Deflaux, N., Bingham, J., Wang, Z.Z., *et al.* (2017). Whole genome sequencing

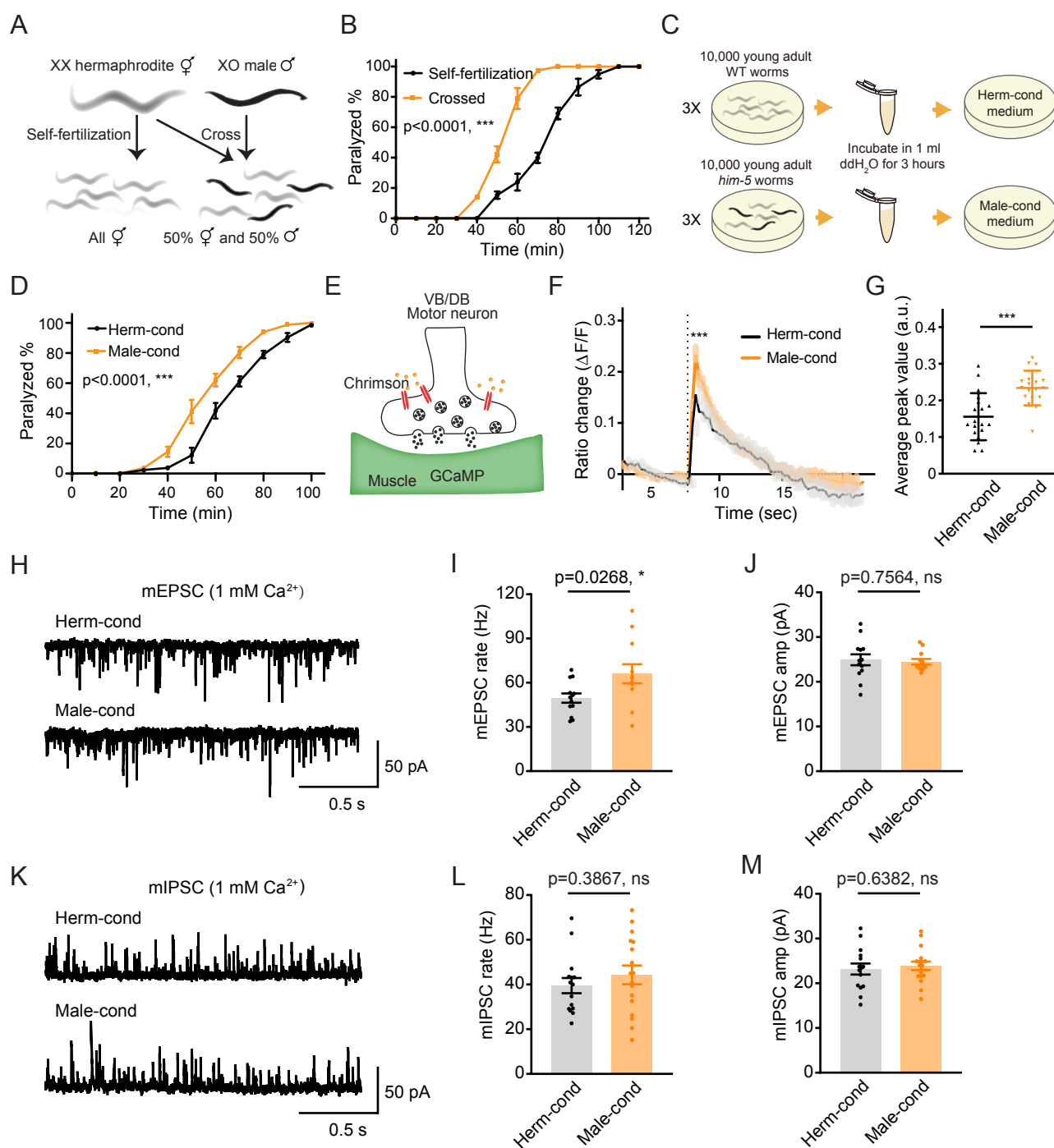
1326 resource identifies 18 new candidate genes for autism spectrum disorder. *Nat Neurosci* 20,
 1327 602-611.

1328 Zamponi, G.W. (2016). Targeting voltage-gated calcium channels in neurological and
 1329 psychiatric diseases. *Nat Rev Drug Discov* 15, 19-34.

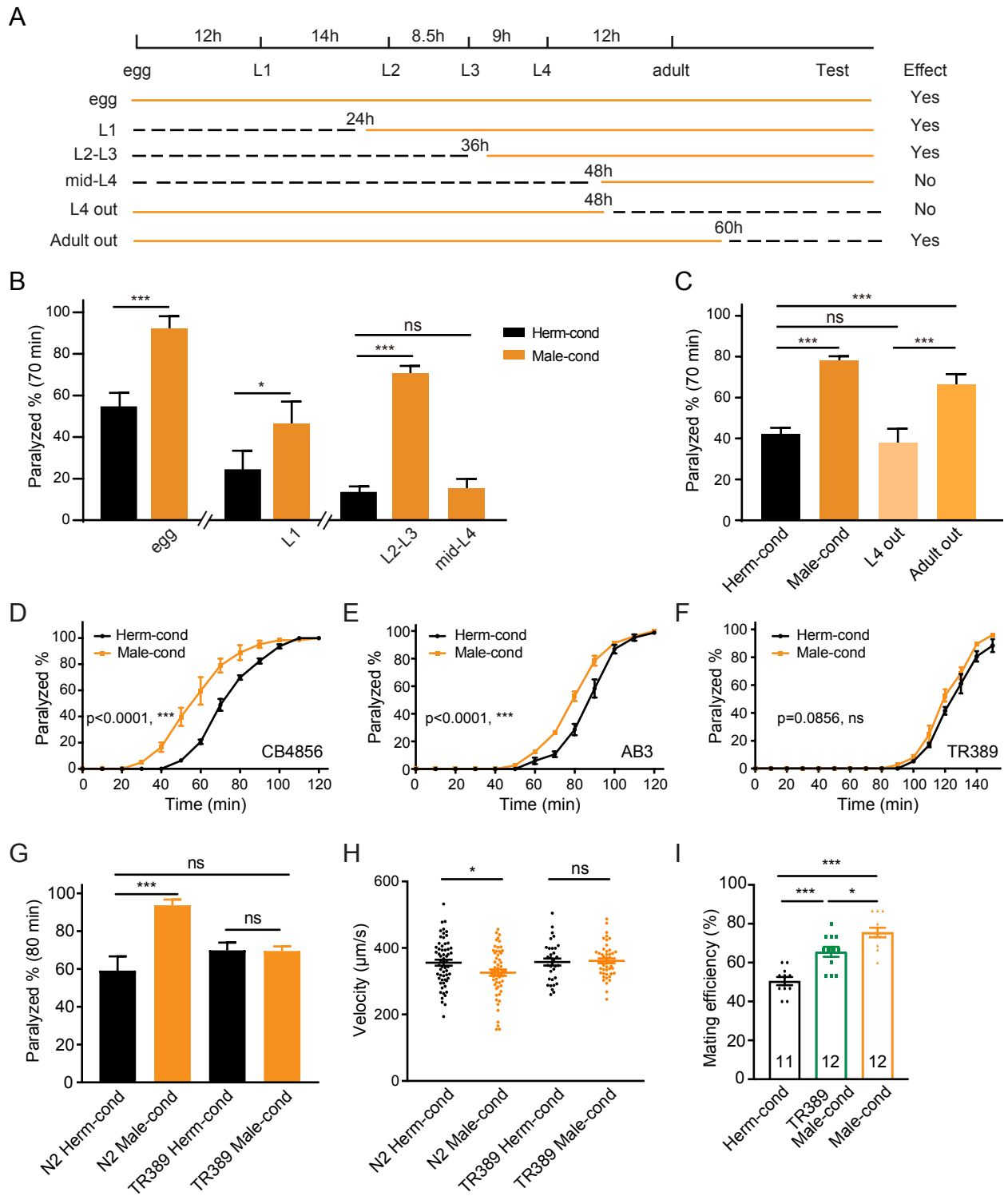
1330 Zhang, X., Noguez, J.H., Zhou, Y., and Butcher, R.A. (2013). Analysis of ascarosides from
 1331 *Caenorhabditis elegans* using mass spectrometry and NMR spectroscopy. *Methods Mol Biol*
 1332 1068, 71-92.

1333 Zhou, Y., Wang, Y.T., Zhang, X.X., Bhar, S., Jones, R.A.L., Han, J., Feng, L.K., and Butcher,
 1334 R.A. (2018). Biosynthetic tailoring of existing ascaroside pheromones alters their biological
 1335 function in *C. elegans*. *Elife* 7.

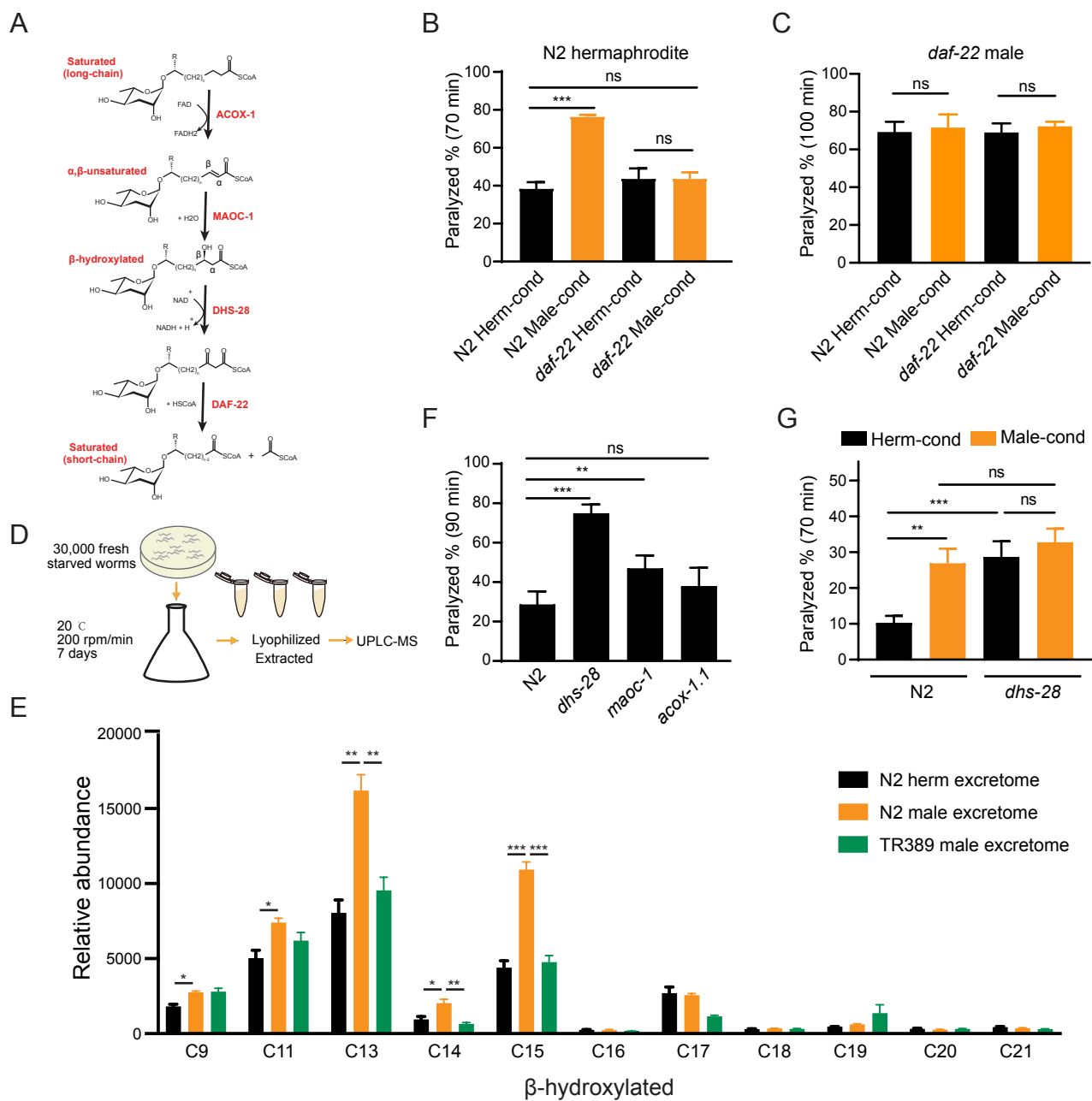
1336 Zou, W.J., Fu, J.J., Zhang, H.N., Du, K., Huang, W.M., Yu, J.W., Li, S.T., Fan, Y.D., Baylis,
 1337 H.A., Gao, S.B., *et al.* (2018). Decoding the intensity of sensory input by two glutamate
 1338 receptors in one *C-elegans* interneuron. *Nat Commun* 9.



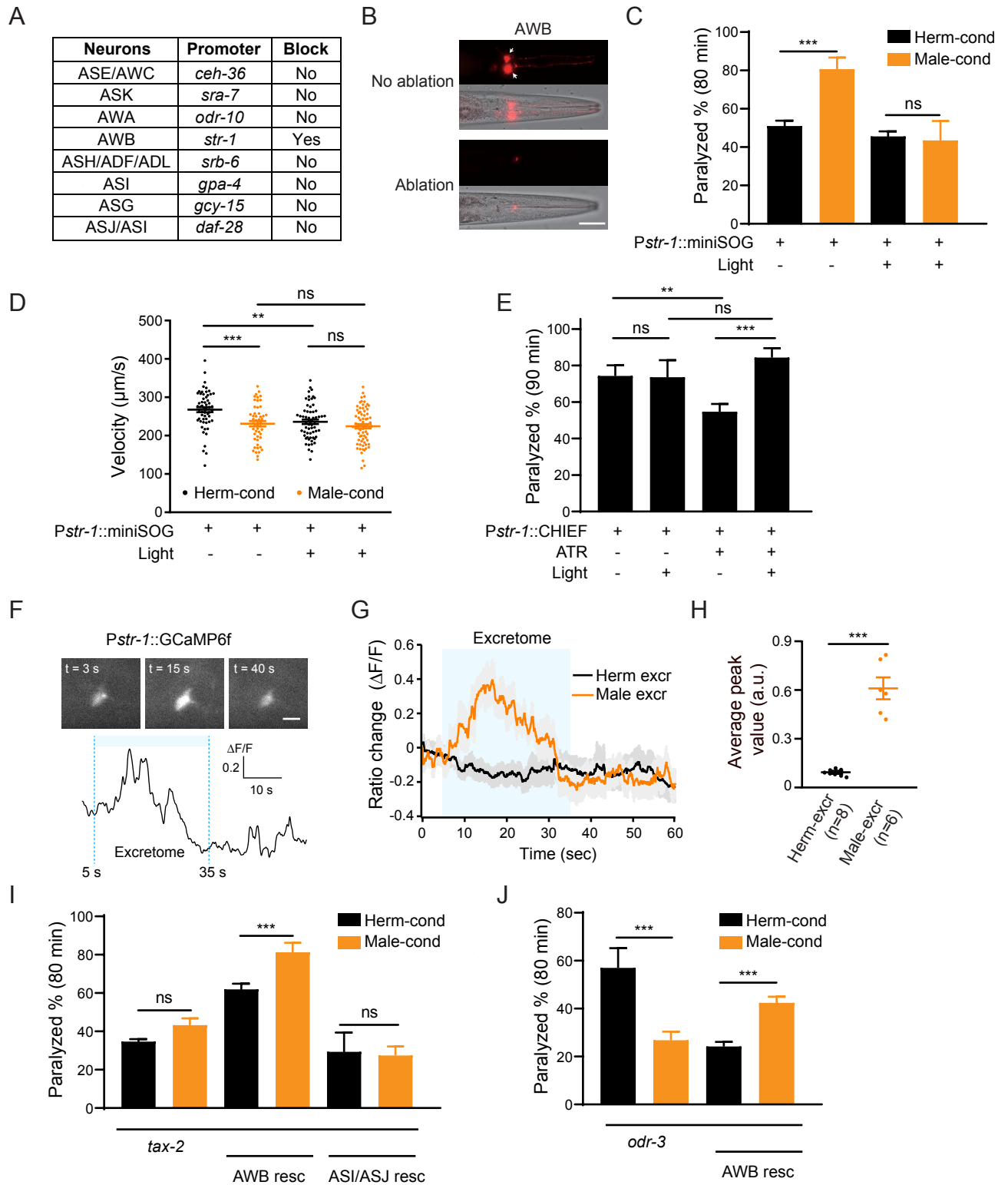
Qian *et al.* Fig. 1



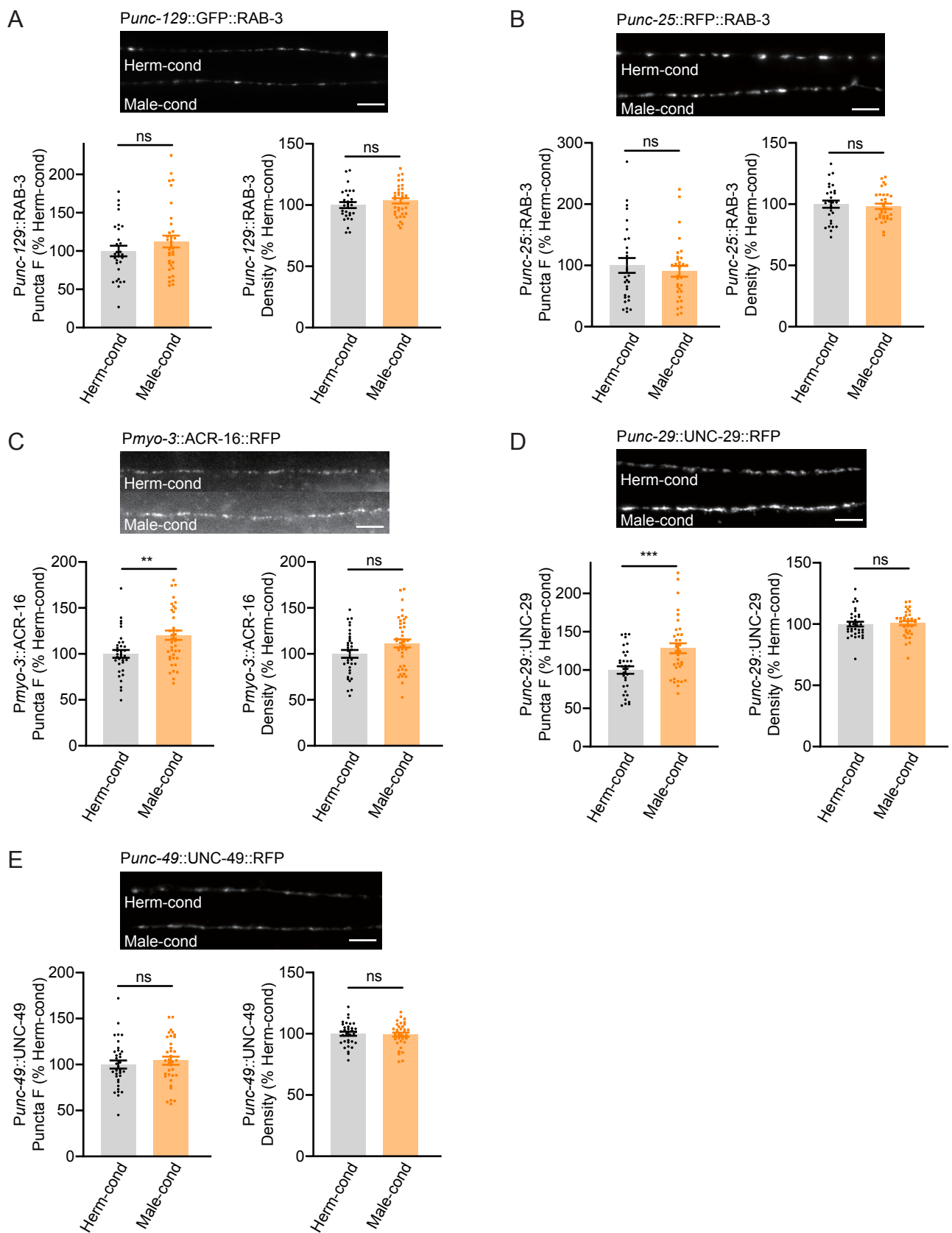
Qian *et al.* Fig. 2



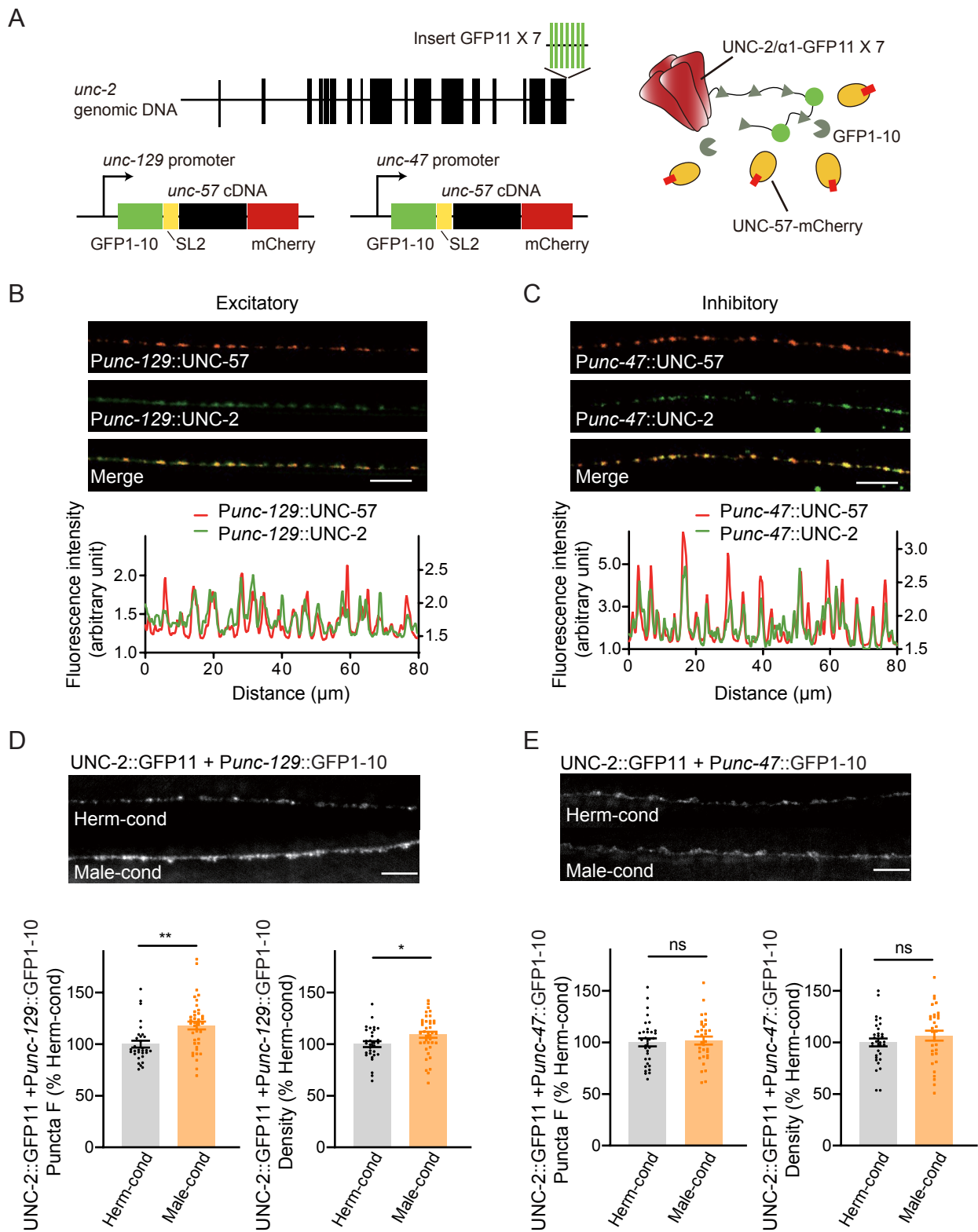
Qian *et al.* Fig. 3



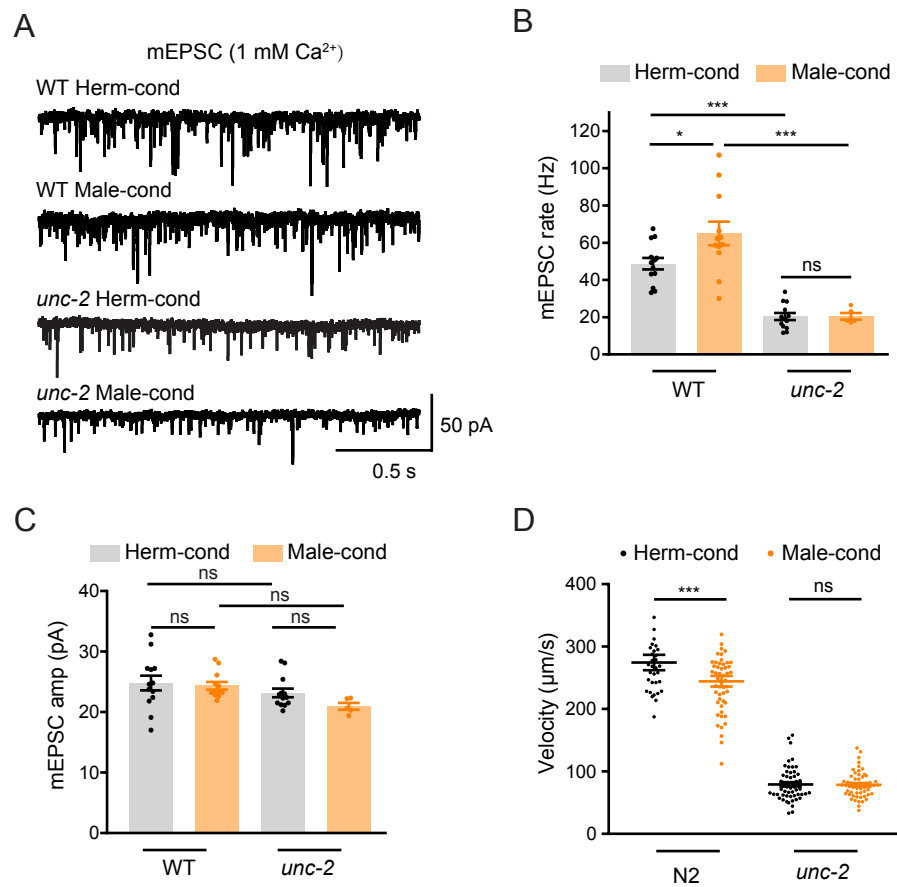
Qian *et al.* Fig. 4



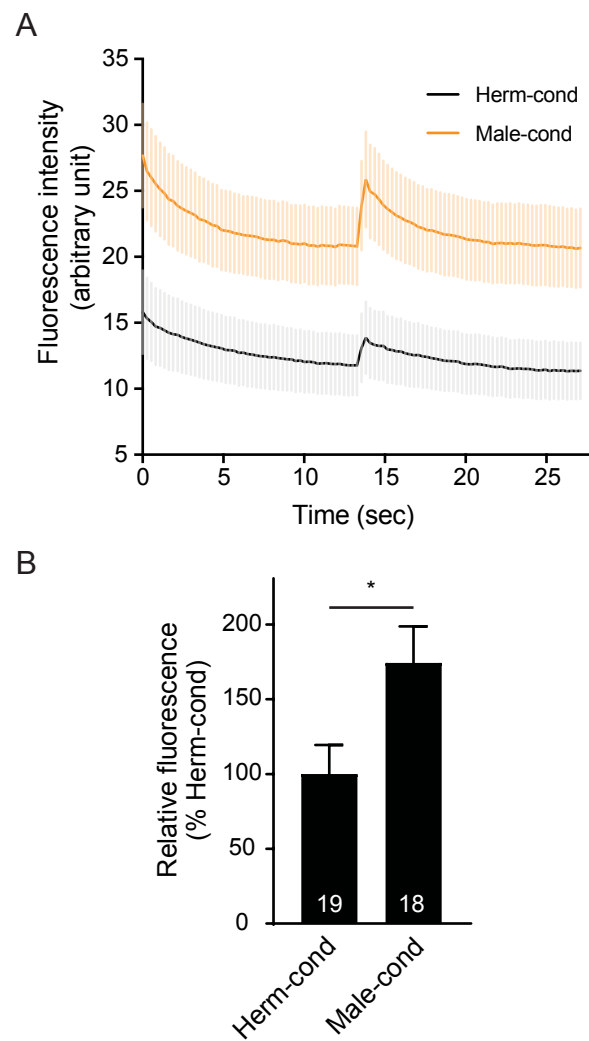
Qian et al. Fig. 5



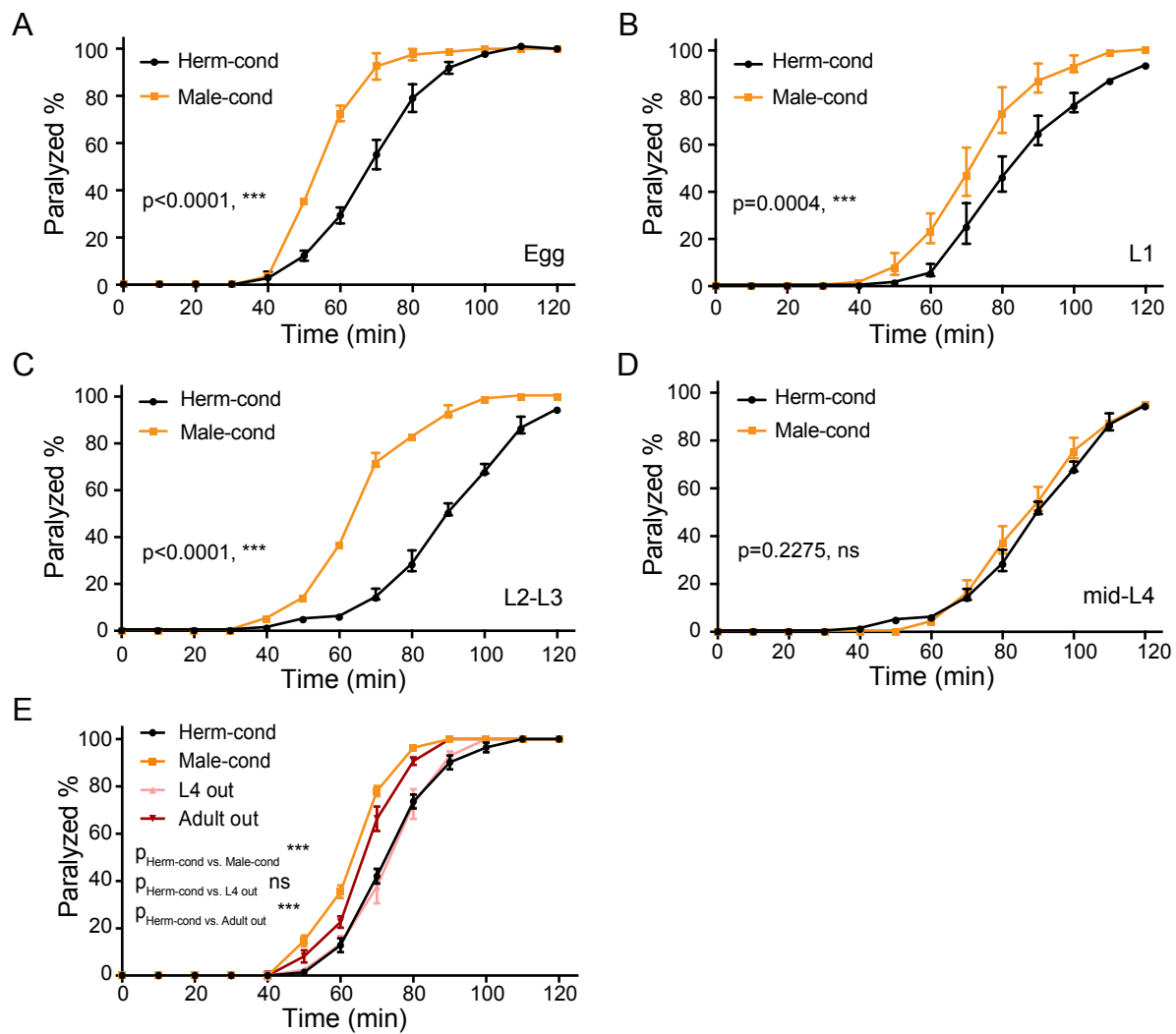
Qian *et al.* Fig. 6



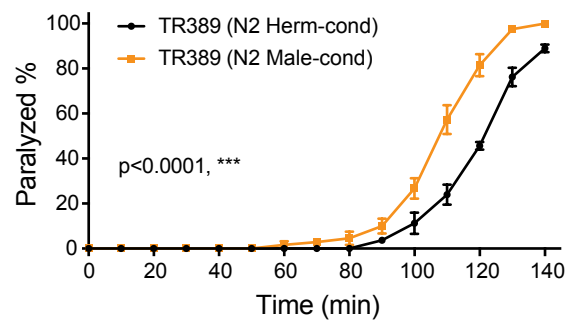
Qian *et al.* Fig. 7



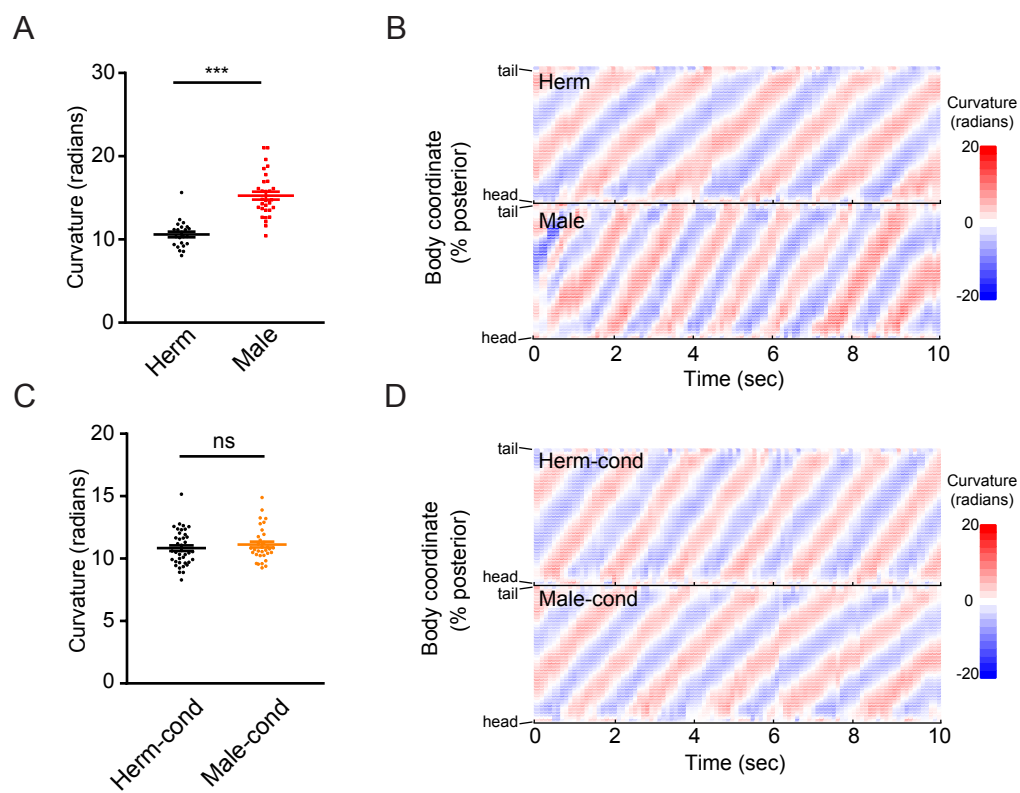
Qian *et al.* Figure 1—figure supplement 1



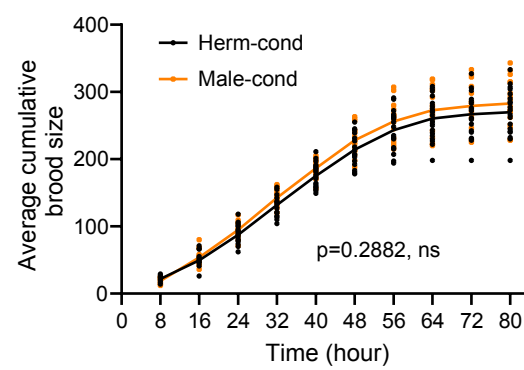
Qian *et al.* Figure 2—figure supplement 1



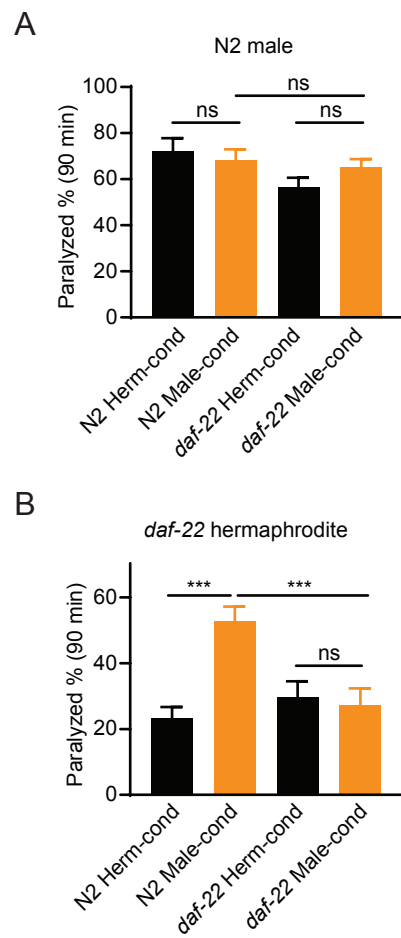
Qian *et al.* Figure 2—figure supplement 2



Qian *et al.* Figure 2—figure supplement 3

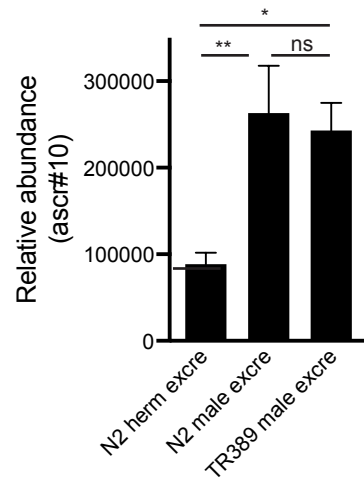


Qian *et al.* Figure 2—figure supplement 4

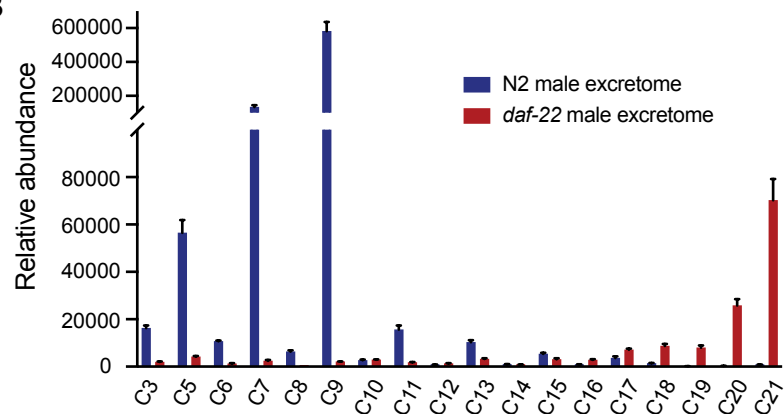


Qian *et al.* Figure 3—figure supplement 1

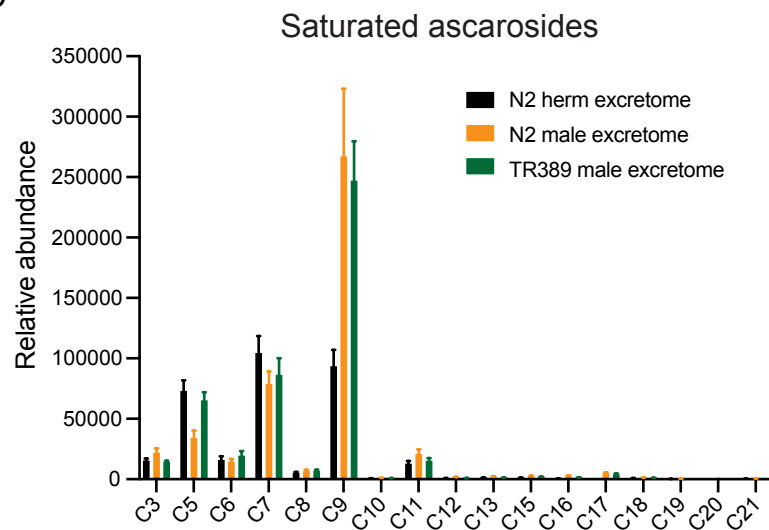
A

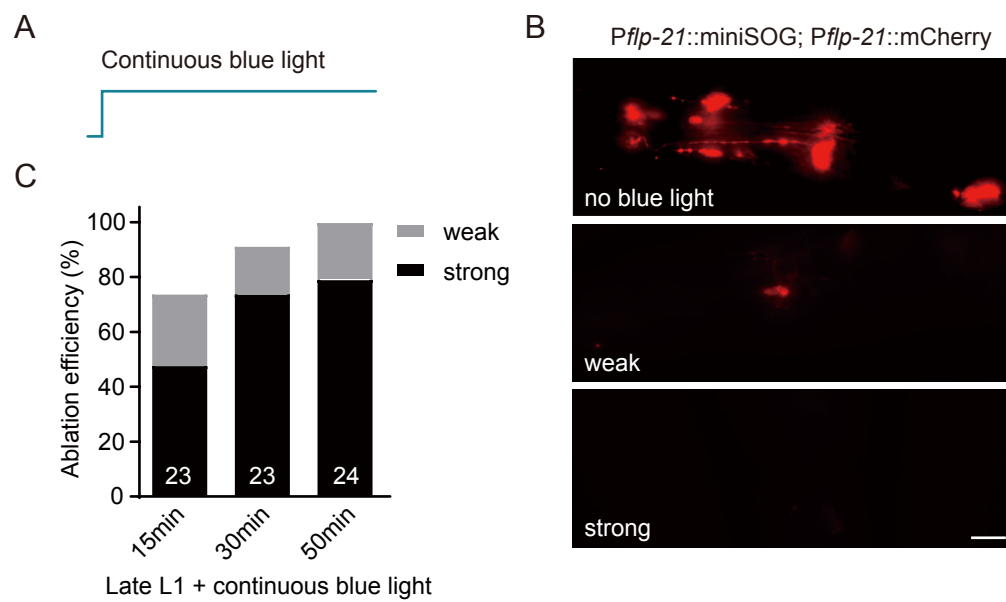


B

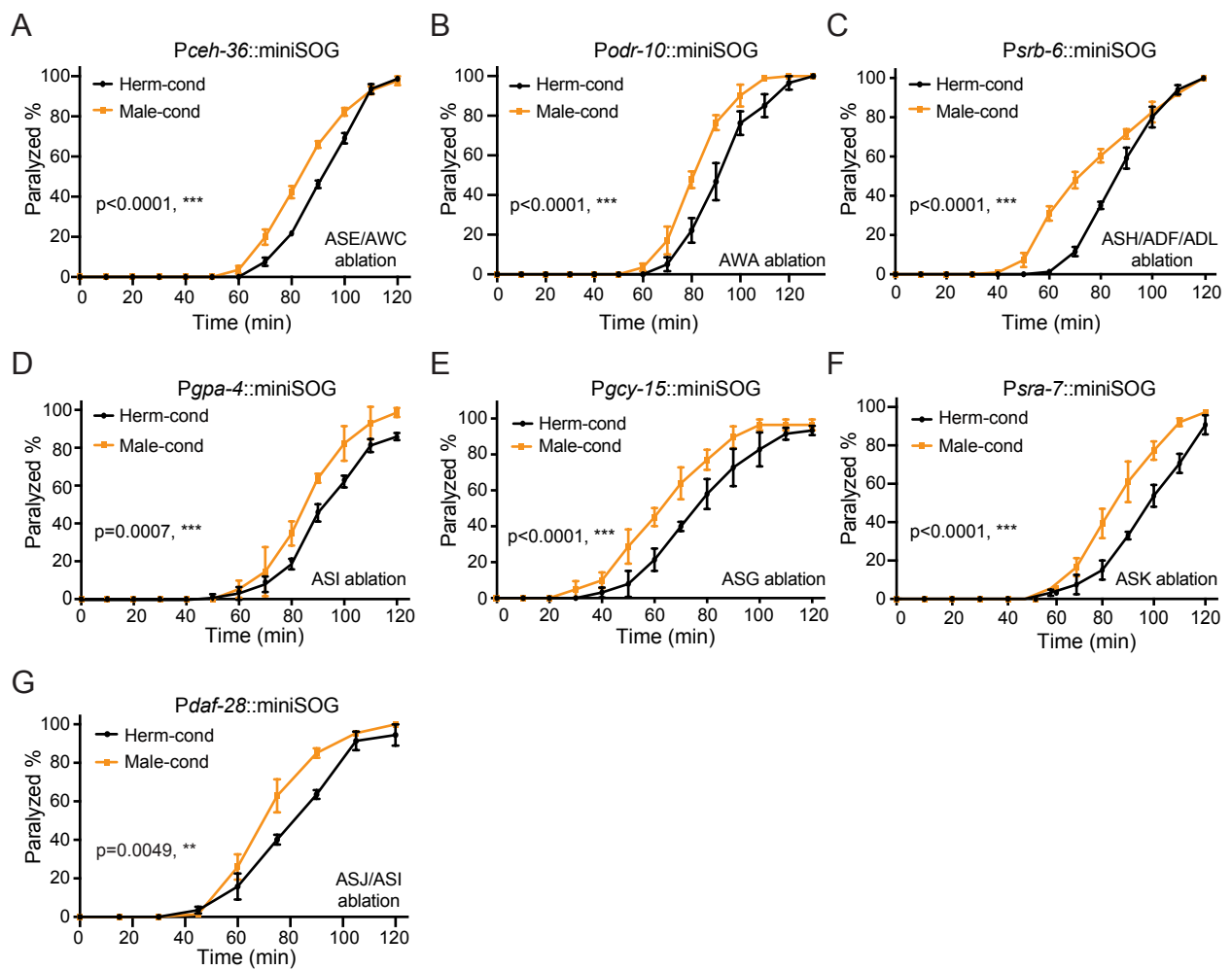


C

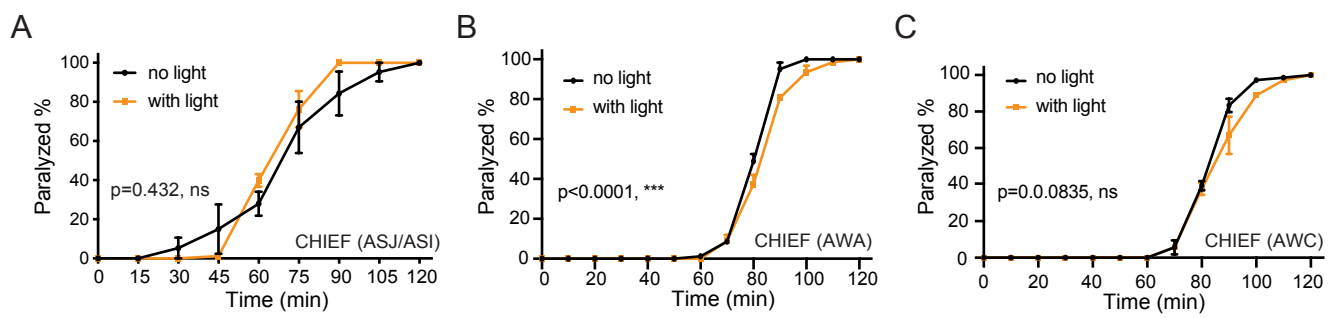




Qian *et al.* Figure 4—figure supplement 1

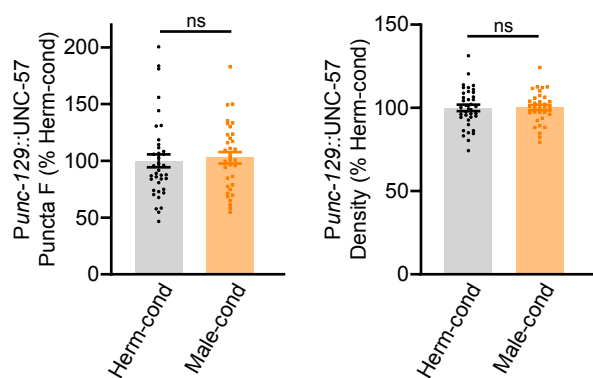
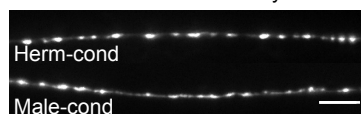


Qian *et al.* Figure 4—figure supplement 2



Qian *et al.* Figure 4—figure supplement 3

A

Punc-129::UNC-57::mCherry

B

Punc-47::UNC-57::mCherry